Characterizing vegetation structural and topographic characteristics sampled by eddy covariance within two mature aspen stands using lidar and a flux footprint model: Scaling to MODIS

L. Chasmer,[1] N. Kljun,[2] C. Hopkinson,[3] S. Brown,[1] T. Milne,[3] K. Giroux,[1] A. Barr,[4] K. Devito,[5] I. Creed,[6] and R. Petrone[1]

Received 30 September 2010; revised 21 March 2011; accepted 28 March 2011; published 23 June 2011.

[1] In this study, a Boolean classification was applied using novel methods to 3-D vegetation structural and topographic attributes found within flux footprint source/sink areas measured by eddy covariance instrumentation. The purpose was to determine if the spatial frequency of 3-D attributes, such as canopy height, effective leaf area index, etc., found within 1 km resolution Moderate Resolution Imaging Spectroradiometer (MODIS) pixels were significantly different from or similar to attributes sampled by flux footprints originating from prevailing wind directions. A Kolmogorov-Smirnov test was used for the first time to apply confidence limits to individual MODIS pixels based on (1) the spatial distribution of cumulative frequencies of attributes representative of those sampled by eddy covariance and (2) temporal representation of MODIS pixels related to area sampling frequency by eddy covariance based on wind direction. Structural and topographic attributes at homogeneous Southern Old Aspen and heterogeneous Upland Aspen sites are representative of 56% and 69% of a 1 km radius area surrounding the tower and 21% and 47% of a 4 × 4 km area. Attributes found within the MODIS "tower" pixel compare well with attributes most frequently sampled by eddy covariance instruments at both sites. By classifying pixels using the Boolean approach, correspondence between MODIS pixels and eddy covariance estimates of gross primary production (GPP) explain up to 13% more variance than using pixels proximal to the tower. This study, therefore, provides a method for choosing MODIS pixels that have similar attributes to those found within footprints most frequently sampled by eddy covariance.

Citation: Chasmer, L., N. Kljun, C. Hopkinson, S. Brown, T. Milne, K. Giroux, A. Barr, K. Devito, I. Creed, and R. Petrone (2011), Characterizing vegetation structural and topographic characteristics sampled by eddy covariance within two mature aspen stands using lidar and a flux footprint model: Scaling to MODIS, *J. Geophys. Res.*, *116*, G02026, doi:10.1029/2010JG001567.

1. Introduction

[2] Exchanges of CO_2 and water are often measured by eddy covariance instruments within relatively homogeneous ecosystems, where the spatial variability of vegetation structural characteristics and ground surface topography is minimal. Scalar fluxes transported from source/sink areas within the 'field of view' of the eddy covariance system are often assumed representative of site average characteristics, regardless of wind direction and atmospheric turbulence. Despite relatively high confidence in the efficacy of measured exchanges within homogeneous ecosystems (barring meteorological and technical problems, etc. For example, see the work of *Baldocchi* [2003]), varying degrees of within site heterogeneity sampled by eddy covariance instruments may not be representative of heterogeneity found within the larger region [*Göckede et al.*, 2008]. Key land cover types may be more heterogeneous than the ecosystems measured by eddy covariance [*Chen et al.*, 1999; *Soegaard et al.*, 2000; *Vourlitis et al.*, 2000]. On the other hand, deployment of eddy covariance instruments within heterogeneous (typical) ecosystems may also result in biased site averages (e.g., because of prevailing wind directions and

[1]Cold Regions Research Centre, Wilfrid Laurier University, Waterloo, Ontario, Canada.
[2]Department of Geography, College of Science, Swansea University, Swansea, UK.
[3]Applied Geomatics Research Group, NSCC, Middleton, Nova Scotia, Canada.
[4]Environment Canada, National Water Research Institute, Saskatoon, Saskatchewan, Canada.
[5]Department of Biological Sciences, University of Alberta, Edmonton, Alberta, Canada.
[6]Department of Biology, University of Western Ontario, London, Ontario, Canada.

0148-0227/11/2010JG001567

sampling of some attributes more than others) [*Scanlon and Albertson*, 2003; *Yoshio et al.*, 2005; *Rebmann et al.*, 2005; *Nagy et al.*, 2006; *Chasmer et al.*, 2008a] or technical limitations of the eddy covariance methodology [*Massman and Lee*, 2002].

[3] The use of flux footprint models has improved understanding of the spatial and temporal distribution of source/sink areas measured by eddy covariance instrumentation, especially as footprints relate to wind speed and direction [*Schmid*, 1994; *Amiro*, 1998; *Finnigan*, 2004; *Rebmann et al.*, 2005; *Vesala et al.*, 2008]. The flux footprint is defined as the probability of flux contribution per unit area upwind of the eddy covariance instrumentation [*Schmid*, 1994; *Kljun et al.*, 2002, 2004]. When combined with remote sensing data, a footprint model provides spatially contiguous information on vegetation structure, topography, and possible source/sink influences on net ecosystem production (NEP) [*Rahman et al.*, 2001; *Rebmann et al.*, 2005; *Kim et al.*, 2006; *Chasmer et al.*, 2008a; *Chen et al.*, 2008]. Further, land surface heterogeneity, which may influence (or "contaminate") flux scalars originating from beyond the homogeneous area of interest may be considered within a time series of flux measurements on the basis of the location of a footprint [*Rebmann et al.*, 2005; *Nagy et al.*, 2006].

[4] With over 500 sites containing eddy covariance and meteorological instrumentation in operation worldwide, assessment of their site representation within ecozones is fundamental for both scaling to larger regions, and understanding fluxes within heterogeneous and/or rapidly changing ecosystems (e.g., such as those found in Europe, the discontinuous permafrost zone of the sub-Arctic, areas undergoing successional changes in vegetation, etc.) [*Göckede et al.*, 2008]. To this end, numerous studies have combined footprint models with eddy covariance data, and in some cases, spectral remote sensing data for quality control [*Aubinet et al.*, 2001; *Rebmann et al.*, 2005; *Nagy et al.*, 2006; *Göckede et al.*, 2008] assessment of biophysical influences on fluxes [*Rannik et al.*, 2000; *Scanlon and Albertson*, 2003; *Yoshio et al.*, 2005; *Chasmer et al.*, 2008a] and scaling [*Soegaard et al.*, 2000; *Vourlitis et al.*, 2000; *Chen et al.*, 2008; *Chen et al.*, 2011]. However, use of moderate to low-resolution spectral remote sensing data sometimes combined with footprint models is not without limitations. Spectral vegetation indices can often be problematic for identifying canopy attributes and complexity [e.g., *Hall et al.*, 1995; *Chen*, 1996; *Franklin et al.*, 1997; *Fassnacht et al.*, 1997; *Treitz and Howarth*, 1999; *Eklundh et al.*, 2001; *Lu et al.*, 2004; *Wang et al.*, 2005]. Further, variability between pixels may or may not be associated with land cover attributes.

[5] In this study, a Boolean classification methodology, often used in spectral remote sensing data analysis, is applied using innovative methods to ranges of 3-D vegetation structural and topographic attributes measured using airborne scanning light detection and ranging (lidar). Structural vegetation and topographic characteristics integrated within footprints originating from prevailing wind directions are used to assess eddy covariance sampling within a 1 km radius of eddy covariance instrumentation within homogeneous and heterogeneous mature boreal aspen stands. The classification is also applied to the local region for assessing the validity of pixel GPP estimated from the Moderate Resolution Imaging Spectroradiometer (MODIS). A Kolmogorov-Smirnov test is used to assign confidence limits for the first time to MODIS pixels based on attribute similarities sampled within the eddy covariance field of view. The test is also used to determine the percent frequency of eddy covariance instrument sampling periods with which each pixel is representative. Therefore, quantification of MODIS pixel characteristics are directly compared with areas most frequently sampled by eddy covariance *not* necessarily representative of the entire 360° 1 km radius area.

[6] The specific objectives of this study are to (1) quantify parts of the ecosystem that are sampled most frequently by eddy covariance instrumentation; (2) assess heterogeneity of vegetation structural and topographic characteristics with increasing distances from eddy covariance instrumentation; (3) use vegetation structural and topographical attributes within footprint source/sink areas to classify site representation within and beyond the a 1 km radius of the eddy covariance system; (4) compare GPP estimated using eddy covariance methods with GPP estimated from MODIS; and (5) assign confidence limits to MODIS pixels.

2. Site Description

[7] The heterogeneous Upland Aspen site was established as part of research on the moraine landform of the Utikuma Region Study Area [*Devito et al.*, 2005; *Ferone and Devito*, 2004; *Petrone et al.*, 2007; *Brown et al.*, 2010] located within the Western Boreal Plains ecozone (Figures 1a and 1c). Eddy covariance instrumentation is situated at the center of three major land cover types, which form a pothole-like hummock-hollow terrain: (1) previously burned (1962) upland composed of mostly trembling aspen, with minimal balsam poplar (*Populus balsamifera*) and white spruce (*Picea glauca*); (2) sparsely treed peatlands comprised mainly of sparse black spruce (*Picea mariana* Mill.), some larch (*Larix laricina*), understory vegetation (Labrador Tea (*Ledum groenlandicum*), and mosses (*Sphagnum* and feathermoss spp.); and (3) ponds which occur in association with peatlands, with peat up to 40 m from the pond edge. Narrow strips of riparian-like vegetation occur at the peat–forestland edge. Mean annual air temperature at Upland Aspen in 2006 (the year of study) was 1.3°C, which is higher than the 1971–2000 mean annual temperature of 0.55°C measured at Slave Lake and cumulative precipitation was 453 mm, which is lower than the 30 year normal (515 mm) [*Petrone et al.*, 2007].

[8] Southern Old Aspen site [*Sellers et al.*, 1997; *Barr et al.*, 2004; *Bernier et al.*, 2006; *Kljun et al.*, 2006] (Figures 1b and 1d) is characterized by a relatively homogeneous forest stand containing mostly trembling aspen, approximately 10% balsam poplar (*Populus balsamifera* L.) and a dense hazelnut (*Corylus cornuta* Marsh.) and green alder (*Alnus crispa* (Alt.) Pursch) understory [*Barr et al.*, 2006]. Mean annual air temperature at Southern Old Aspen in 2008 (the year of study) was 1.2°C, which is higher than the 1971–2000 mean annual temperature of 0.4°C measured nearby at Waskesiu Lake (Environment Canada).

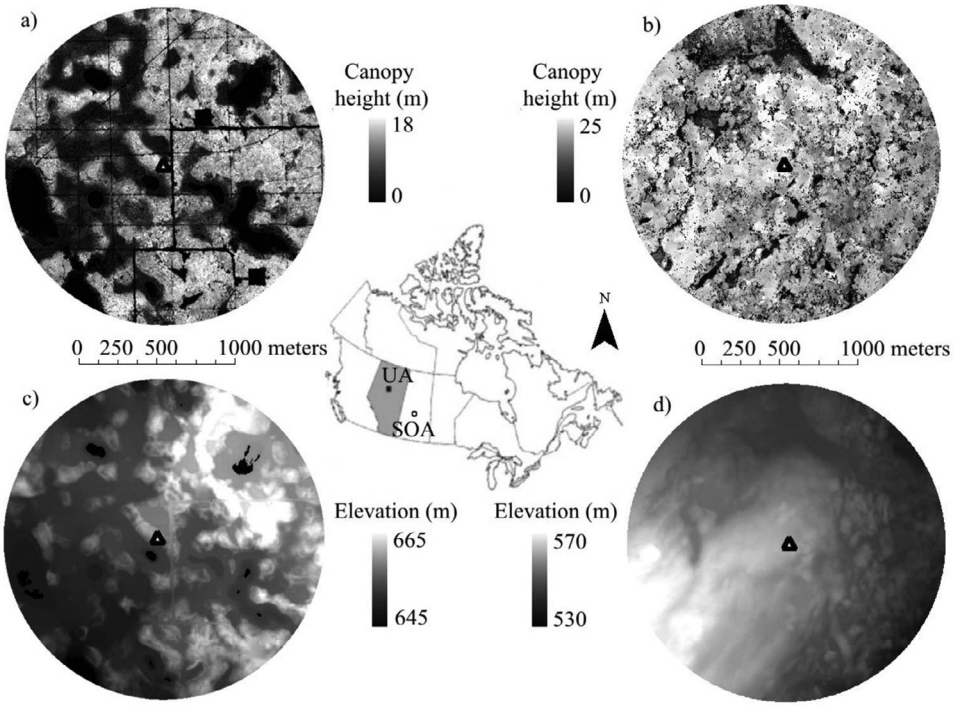

Figure 1. Location of Southern Old Aspen (SOA) and Upland Aspen (UA) sites in Saskatchewan and Alberta, Canada. (a) Canopy height and (c) elevation within 1 km radius of the eddy covariance tower at Upland Aspen. (b) Canopy height and (d) elevation within 1 km radius of the eddy covariance tower at Southern Old Aspen. Black patches in Figure 1c are missing data because of absorption (or specular reflection at wide scan angles) of laser reflections by water.

Cumulative precipitation was 398 mm, which is lower than the 30 year normal (467 mm).

3. Data Collection

3.1. Eddy Covariance Instrumentation and Data Processing

[9] Eddy covariance instrumentation and data processing methodologies for both sites are summarized in Table 1. Half-hourly gross ecosystem production (GEP) estimates from eddy covariance data were examined from 10 June to 28 July 2006 and 2008 at Upland Aspen and Southern Old Aspen, respectively (August not examined because of missing data at Southern Old Aspen) (Table 1). GEP was compared with MODIS GPP at both sites, assuming that GPP and GEP are analogous (even though they are not identical [*Goulden et al.*, 1996]). GEP (herein referred to as GPP) was estimated per half-hourly period during the day from net ecosystem production (NEP) and ecosystem respiration (Re) (GPP = NEP − Re). At Southern Old Aspen and Upland Aspen, nighttime periods of Re = NEP when photosynthesis was zero. During the daytime, Re was determined using an empirical model based on temporal variability of soil temperature (T_{soil}) at 2 cm depth or air temperature (T_{air}) measured at a height approximating two thirds of the canopy height [e.g., *Griffis et al.*, 2003; *Barr et al.*, 2006]. GPP data gaps were filled using flexible moving window approaches at Southern Old Aspen [*Barr et al.*, 2004] and 14 d means at Upland Aspen [*Falge et al.*, 2001]. Average energy balance closure (Le + H/Rn − Qg, where Qg is ground heat flux and Rn is net radiation) for periods studied was 79% (Southern Old Aspen), and 76% (Upland Aspen).

3.2. Overview of Footprint Methodology

[10] A simple flux footprint parameterization [*Kljun et al.*, 2004] was used to estimate temporally varying (30 min) contribution areas and associated vegetation and topographical characteristics to eddy covariance instrumentation. The parameterization is based on a full-scale Lagrangian particle model [*Kljun et al.*, 2002], valid for a broader range of atmospheric conditions than analytical methods [*Schmid*, 2002], but does not require the computing resources needed by more complex numerical models [e.g., *Foken and Leclerc*, 2004]. Measurements of wind direction, the height of the eddy covariance system (z), height of the planetary boundary layer (h), roughness length of vegetation (z_0), the standard deviation of the vertical wind velocity (σ_w), and friction velocity (u^*) were incorporated into the parameterization [*Kljun et al.*, 2004]. Richardson number (Ri) was used to approximate average atmospheric stability from T_{air} and wind speed per half-hourly period [*Monteith and Unsworth*, 1990]. Tables from the work of *Gryning et al.* [1987] were used to approximate h based on a generalized stability factor estimated from Ri. Airborne lidar data were used to estimate z_0 and zero plane displacement (d) based simply on canopy height (z_0 = 1/10 height, d = 2/3 height) [*Oke*, 1996]. These (z_0 and d) were averaged within

Table 1. Meteorological and Eddy Covariance (EC) Instrumentation and Data Processing Specifications

Eddy Covariance Instrumentation/Data Processing Specifications	Southern Old Aspen (References)	Upland Aspen (References)
EC make and model of instruments below		
- Sonic anemometer	Model R3 Gill Instruments, Ltd.	CSAT3, Campbell Scientific Inc.
- Infrared gas analyzer	Model LI 6262, LI-COR Inc.	Model LI 7500, LI-COR Inc.
- Type (open/closed)	Closed path [*Barr et al.*, 2006]	Open path
EC measurement frequency (Hz)	20	20
Height of EC instruments (m)	39	25.5
Measured exchanges[a]	H, Le, F_{NEE}, $u*$ [*Barr et al.*, 2006]	H, Le, F_{NEE}, $u*$
$u*$ threshold (m s^{-1})	0.35	0.35 [*Petrone et al.*, 2007]
Correction procedures used	Standard gap filling using flexible moving window [*Griffis et al.*, 2003; *Barr et al.*, 2004, 2006].	Rotation of vertical and horizontal wind velocities to zero [*Kaimal and Finnigan*, 1994]. Gap filling based on mean for 14-day periods [*Falge et al.*, 2001].
Flux partitioning procedures	F_{NEE} = sum of EC flux at height z (39 m) and rate of change of CO_2 storage in air column below z [*Barr et al.*, 2006]. R = F_{NEE} at night, adjusted for T_{soil} or T_{air} [*Griffis et al.*, 2003; *Barr et al.*, 2004, 2006].	F_{NEE} = sum of EC flux at height z (25.5 m) and rate of change of CO_2 storage in air column below z R = F_{NEE} at night, adjusted for T_{soil} [*Griffis et al.*, 2003].
Application of surface energy balance closure adjustment to EC data	Adjustment applied [*Barr et al.*, 2006]	Adjustment applied [*Barr et al.*, 2002; *Finnigan et al.*, 2003]

[a]Measured exchanges are sensible heat exchanges (H), latent heat exchanges (Le), net ecosystem exchange (F_{NEE}), friction velocity ($u*$). R, ecosystem respiration; T_{soil}, soil temperature at 2cm depth; T_{air}, at two-thirds canopy height.

10 degree wind sectors starting at 0 degrees (north), and extending up to 100 m from the eddy covariance instrumentation. z_0 and d were applied at half-hourly periods to the footprint parameterization depending on wind direction.

[11] Changes in $u*$ and h can influence the length of footprints, whereby increased $u*$ and decreased h can result in footprint shapes centering on areas closer to the eddy covariance instrumentation (and vice versa). In areas of heterogeneity and variable land surface patches, such as those found at Upland Aspen, the use of this model might be somewhat problematic. Footprint models such as Large Eddy simulation (LES) [*Foken and Leclerc*, 2004] might more accurately account for boundary layer turbulence created by patches. However, these will be too computationally intensive for real-time application of the model at half-hourly periods throughout the growing season at two sites. Concentration on a few key periods would limit the scalability of the eddy covariance sampling and land cover classification, unless all scalar directions and ranges of atmospheric turbulence could be accounted for (which may exceed seasonal period applications of the model, anyways). Despite these limitations, the parameterization used in this study provides an approximate estimate of the source/sink area in question as well as the location of the maximal contribution to the measured flux.

3.3. Lidar Data Collection and Processing

[12] Airborne lidar surveys were parameterized, and data were collected and processed by the authors during the Upland Aspen and Southern Old Aspen campaigns on 28 August 2002 and 3 August 2008 (Table 2). Flux measurements were approximately coincident with the lidar survey at Southern Old Aspen, and four years following the lidar survey at Upland Aspen. A subtraction of canopy heights at Upland Aspen between August 2002 lidar data collection and a repeat collection in 2008 illustrate minimal average growth of <0.75 m in mature mixed wood upland stand near the site and <0.62 m height increase in peatland areas associated with open water where sites have not been previously disturbed. The Upland Aspen site was harvested in 2007. Lidar-derived data layers of vegetation structural characteristics and topography used in subsequent analyses are described in Table 3.

3.4. MODIS

[13] The MODIS GPP product (MOD17) has a global 1 km pixel resolution with an 8 d cumulative repeat time and is intended for seasonal to interannual assessment of global vegetation productivity. The algorithm, described by *Running et al.* [2004], incorporates MODIS-estimated fraction of PAR absorbed by the canopy (FPAR) and leaf

Table 2. Lidar Survey Specifications at Southern Old Aspen and Upland Aspen

Lidar Specifications	Southern Old Aspen	Upland Aspen
Model number of reflections per pulse	ALTM 3100 (Optech Inc. Toronto, Canada) 4	ALTM 2050 (Optech Inc.) 2
Flying height above ground level (m)	~700 m	~1200 m
Scan angle from nadir (°)	±20	±16
Pulse repetition frequency (kHz)	70	50
Percent overlap of scan lines	50	50
Density of returns with 50% overlap	≤25 per m^3	≤12 per m^3

Table 3. Three-Dimensional Canopy Structural and Topographic Layers Integrated With the Results of a Footprint Model and Used for Classifying Same Vegetation Topographic Attributes Beyond a 1 km Radius Surrounding Eddy Covariance Instruments

Canopy Structural or Topographical Metric	Lidar Data Product	Methodology	Reference
Elevation (m)	Digital elevation model (DEM)	Inverse distance weighting algorithm (IDW) of ground-classified laser reflections at 1 m	*Hopkinson et al.* [2005]
Canopy height (m)	Canopy height model (CHM)	Mean maximum canopy height using IDW algorithm within a 2.5 m search radius of classified canopy reflections >0.5 m above the ground.	*Hopkinson et al.* [2005]
Canopy surface (elevation + canopy height) (m)	Digital surface model (DSM)	Digital surface model = elevation + canopy height (m)	*Hopkinson et al.* [2005]
Canopy fractional cover (%) below understory	$f\text{cover}_{50}$ at 0.5 m above ground	Beer's Law laser intensity method, where *f*cover $= 1 - \left(\frac{\left(\frac{\Sigma I_{GroundSingle}}{\Sigma I_{Total}}\right) + \sqrt{\frac{\Sigma I_{Groundsingle}}{\Sigma I_{Total}}}}{\left(\frac{\Sigma I_{First} + \Sigma I_{Single}}{\Sigma I_{Total}}\right) + \sqrt{\frac{\Sigma I_{Intermediate} + \Sigma I_{Last}}{\Sigma I_{Total}}}} \right)$ where I = reflection intensity, and "First," etc., refers to the order of reflections per pulse.	*Hopkinson and Chasmer* [2009]
Canopy fractional cover (%) above 1.3 m (height of validation)	$f\text{cover}_{130}$ at 1.3 m above ground		
Effective leaf area index ($m^2\ m^{-2}$) above understory	LAIe_{130}	$\text{LAIe} = -\ln\left(\frac{1-f\ \text{cover}}{k}\right)$ where k = extinction coefficient (0.5 used for both sites).	*Morrison et al.* [2010]
Effective leaf area index ($m^2\ m^{-2}$) below understory	LAIe_{50}		
Uplands and Lowlands	Uplands and lowlands	Ratio of uplands (1) to lowlands (−1) and zero change (0) determined using a low-pass 100 m resolution filter of the DEM (to identify <100 m area landscape depressions found at Southern Old Aspen and Upland Aspen) and the residual deviation (at 1 m resolution) from the low-pass surface.	This study
Zero plane displacement (m)	d	5 m resampled 2/3 canopy height (from CHM)	This study
Roughness length (m)	z_0	5 m resampled 1/10 canopy height (from CHM)	This study

area index (LAI) (MOD15) with incoming PAR, minimum T_{air} (24 h), and daytime average vapor pressure deficit (VPD) modeled using a general circulation model (NASA Data Assimilation Office (DAO)). Maximum biome-specific light use efficiency (LUE) is varied based on T_{air} and VPD to arrive at a daily LUE estimate used in the GPP calculation. Daily LUE is multiplied by APAR (APAR = FPAR * PAR) to estimate daily GPP.

[14] MOD17A2 (collection 5) [*Zhao et al.*, 2005; *Heinsch et al.*, 2006; see also MODIS daily photosynthesis (Psn) and annual net primary production (NPP) product (MOD17), Theoretical basis document, Version 3, 1999, http://modis.gsfc.nasa.gov/data/atbd/atbd_mod16.pdf] data were obtained for a 4 km × 4 km area from DOY 152 to 209 2006 (Upland Aspen) and 2008 (Southern Old Aspen), coincident with eddy covariance GPP estimates. Data were provided in GeoTIFF format (WGS84, reprojected to UTM NAD83) from Oak Ridge National Laboratory (ORNL) Distributed Active Archive Center (DAAC).

4. Analytical Methods

4.1. Site Variability: Increasing 10 m Radius Domain Areas

[15] Concentric rings centered on eddy covariance instrumentation at Southern Old Aspen and Upland Aspen are used to determine average and ± σ structural and topographic characteristics within increasing (10 m radius) areas surrounding the tower. The purpose is to determine the distance at which average structural and topographic differences begin to increase. The location of the maximum probability of flux, determined from the footprint probability density

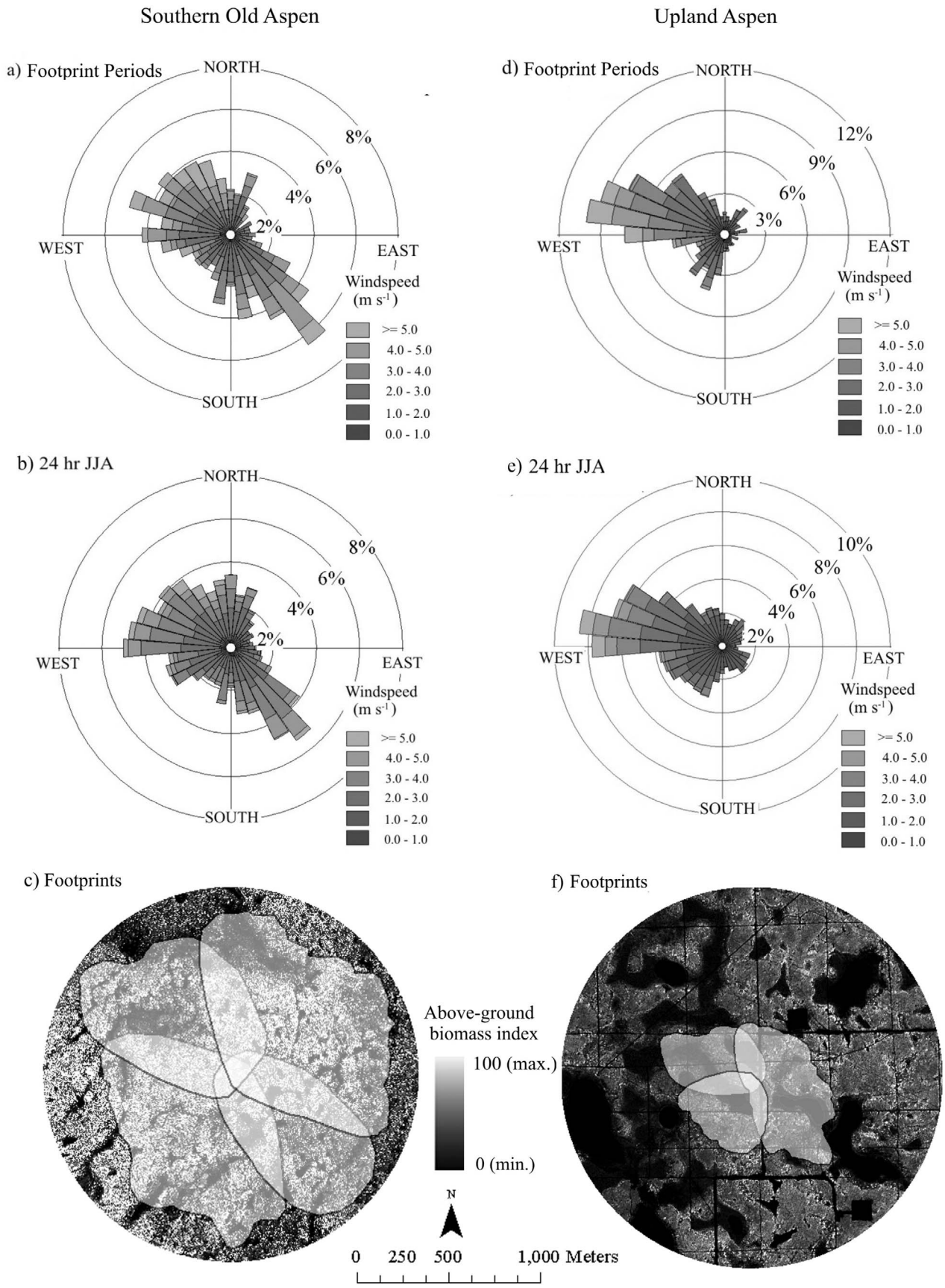
Southern Old Aspen
Upland Aspen
a) Footprint Periods
d) Footprint Periods
NORTH
SOUTH
WEST
EAST
2%
4%
6%
8%
3%
6%
9%
12%
Windspeed (m s-1)
>= 5.0
4.0 - 5.0
3.0 - 4.0
2.0 - 3.0
1.0 - 2.0
0.0 - 1.0
b) 24 hr JJA
e) 24 hr JJA
2%
4%
6%
8%
10%
c) Footprints
f) Footprints
Above-ground biomass index
100 (max.)
0 (min.)
N
0 250 500 1,000 Meters

Figure 2

function (x_{max}) (average distance = 82 m and 78 m from the tower at Southern Old Aspen and Upland Aspen) was used as a baseline for comparison. This assumes that the location at x_{max} represents 3-D attributes that have the highest probability of sampling by eddy covariance instrumentation.

4.2. Lidar Data/Footprint Integration

[16] Lidar data layers were extracted from within footprints at half-hourly periods to determine: a) within-site structural vegetation and topographic characteristics most frequently sampled by eddy covariance instrumentation; and b) ranges of vegetation and topographic characteristics from frequently sampled areas used to inform a local-scale classification. The areal extent in x and y directions of the source/sink areas determined from the modeled footprint were converted to Universal Transverse Mercator (UTM) coordinates for integration with lidar data layers [*Chasmer et al.*, 2008a]. Source weight functions up to the 80% probability density function level were used to identify grid cells (pixels) within the footprint that corresponded to 1 m resolution gridded lidar data products. All vegetation and topographical characteristics within the 80% footprint probability density function were treated equally, therefore source weights were not applied. A sensitivity analysis was used to compare weighted versus unweighted (linear averages) of within footprint attributes (canopy height, elevation, $LAIe_{50}$ and the ratio of uplands to lowlands) from prevailing wind directions. The results of the sensitivity analysis indicate that attributes within weighted versus unweighted footprints are not significantly different at the Upland Aspen site, except for the case of the ratio of uplands to lowlands, which are influenced by upland/lowland positioning but have little influence on MODIS spectral bands (because of the overhead canopy). At Southern Old Aspen, significant differences in $LAIe_{50}$ occur between weighted versus unweighted footprints originating from prevailing wind directions. This is due to the location of a large wetland located in the area of the maximum weighting (x_{max}). The use of reduced LAIe within the classification because of the influence of the wetland will limit classified areas and may not be representative of LAIe within closer proximity of the eddy covariance instrumentation (also within the range of x_{max}). Other attributes from prevailing wind directions were not significantly different at Southern Old Aspen, and therefore we have decided not to weight footprints for MODIS pixel classification. The maximum footprint extent was limited to 80% for optimal performance of the model [*Kljun et al.*, 2004]. At 90%, *Kljun et al.* [2004] show a significant flattening of the probability density function curve and reduced performance of the parameterization. Numerous statistics were produced including: average, maximum, minimum and standard deviation of all pixels, per lidar data layer within each footprint.

[17] Footprint/lidar data integrations were applied between 10:00 and 16:30 (local time) at half-hourly intervals. This shortened daytime period was used to avoid uncertainties in flux storage within the air column below the eddy covariance during stable atmospheric conditions [*Yang et al.*, 1999; *Massman and Lee*, 2002]. Periods of low u^* (<0.2 m s^{-1}) were excluded, as well as periods measured during precipitation events, and when the σ of wind vectors per half-hour period exceeded 45°. Only measured turbulence (nongap-filled) was used in the footprint classification analysis. Of the total number of half-hourly footprint periods used at Southern Old Aspen, 14% of half-hourly periods were excluded. At Upland Aspen 6% were excluded. The period of time of footprint extraction, although shortened from daytime GPP periods compared with MODIS, does not affect the GPP comparison because prevailing wind directions over 24 h versus footprint period extractions did not vary greatly (Figure 2).

4.3. Local to Regional Scaling: Lidar-Based Classification Using Within-Footprint Attributes

[18] Each footprint has a unique 'signature' of vegetation structural and topographical attributes sampled by eddy covariance. Attribute ranges within half-hourly footprints originating from prevailing wind directions were classified within and beyond a 1 km radius of the tower. Ranges of vegetation and topographical attributes were individually identified as the mean ± σ of each 3-D attribute (e.g., canopy height, LAIe, etc.) from footprints (n footprints from prevailing wind directions = 318, Southern Old Aspen; 664, Upland Aspen). Three-dimensional data layers were then combined within a Boolean classification of layer intersection. All pixels within the range of attributes per layer (e.g., all canopy heights for all other areas that have ranges between mean ± σ found within footprints originating from prevailing wind directions) were given an identifier of 1 (true). Those outside of that range were given an identifier of zero (false). Any pixels that contained one or more "false" layers were excluded from the wider area classified. All layers were treated equally in the classification.

[19] Table 4 shows mean ± σ ranges of vegetation structural and topographic characteristics within footprints originating from prevailing wind directions compared with 1 km site averages for Southern Old Aspen and Upland Aspen. Lidar data layers (Table 3) used in the classification include: elevation, canopy height, effective below understory leaf area index ($LAIe_{50}$), and percent uplands to lowlands based on a 100 m × 100 m low-pass filter.

4.4. MODIS Pixel Evaluation

[20] Eight-day MODIS GPP was compared with 8 d cumulative (gap-filled) GPP observed throughout each day using eddy covariance instrumentation. MODIS GPP comparisons were made using pixels that contained >50% coverage of structural and topographic attributes determined by the Boolean classification. This quantifies the percentage of pixels that are representative of characteristics sampled by eddy covariance instrumentation, for scaling and validation purposes. The lidar pixel domain resolution used for

Figure 2. Frequency of wind directions and wind speed at (a) Southern Old Aspen during footprint periods studied and (b) at half-hour intervals over 24 h, June, July, and August 2008. (c) Combined footprint areas grouped into prevailing and low-frequency wind origins used within the classification overlaid onto an index of aboveground biomass estimated from canopy height times LAIe50 (unitless) at Southern Old Aspen. (d, e, f) Same as Figures 2a–2c but for Upland Aspen.

Table 4. Vegetation Structural and Topographic Characteristics Based on Mean Maximum and Minimum Standard Deviations Characteristic of Footprints Originating From Prevailing Wind Directions[a]

Lidar-Derived Attributes	Southern Old Aspen Attribute Range Applied	Southern Old Aspen Site Average	Upland Aspen Attribute Range Applied	Upland Aspen Site Average
Elevation (m)	550 – 565	555	653–660	655
Canopy height (m)	9.7 – 25.5	13.2	2.82 – 18.2	7.97
Canopy LAIe below understory, including canopy	0.23 – 7.75	3.28	1.18 – 6.7	2.65
Ratio of uplands to lowlands (between 0 and 1) based on 100 m low-pass filter where < 0 = more lowlands and > 0 = more uplands[b]	−0.03 – 0.60	−0.03	−0.2 – 0.67	−0.10

[a]Site average characteristics are also included for comparison.
[b]Uplands and lowlands are also illustrated on maps.

comparison with 1 km resolution MODIS pixels is 1 m. Pixels obtained during periods of poor quality control were included to demonstrate improvements to GPP when other pixels with similar 3-D attributes were substituted.

4.5. Applying Confidence Limits to MODIS Pixels Based on Footprint Sampling

[21] A Kolmorogov-Smirnov test was used to assign confidence limits to MODIS pixels based on differences between within pixel 3-D attributes and those sampled by eddy covariance instruments. The Kolmogorov-Smirnov test is applied such that comparisons are made between spatial cumulative frequency distribution of individually binned 3-D attributes within a) footprint sampling areas and b) classified MODIS pixels. Attributes included in the test were: canopy height (binned at 0.5 m intervals), $LAIe_{50}$ (binned at 0.25 m^2 m^{-2} intervals), and elevation (binned at 1 m intervals). Other attributes such as uplands and lowlands and existence of understory were not included because they have been divided into binary ratios. The footprint 'domain' area (from which attribute frequencies were cumulated) was determined by tracing the area around all footprints originating from within a range of wind direction vectors. Wind direction vectors were divided into prevailing, secondary peaks, and infrequently sampled areas based on natural breaks in wind direction frequencies. Vegetation structural/elevation attributes were then extracted in the same manner as they were from footprints (but from one large irregular polygon, instead of several hundred footprints) and weighted equally. The cumulative frequency of attributes found within footprint domain areas were then compared with the same cumulative frequency of attributes found within individual MODIS pixels. H_0 assumes that canopy height, or $LAIe_{50}$ or elevation from prevailing wind directions are not significantly different from (1) that found in footprints originating from other wind direction domains (e.g., secondary peaks) or (2) that found in MODIS pixels with >50% coverage of Boolean classified lidar data layers. If they are significantly different, then H_0 is rejected. This provides confidence limits to MODIS pixels whereby p values of 0.01 and 0.05 indicate that there is very little similarity between the attributes sampled by eddy covariance instruments and those found within individual MODIS pixels (H_A). Nonsignificant p values >0.1 indicate that H_0 cannot be rejected (therefore similarities exist).

5. Results

5.1. Frequency Distribution of Source/Sink Contributions to Eddy Covariance

[22] Prevailing wind vectors at Southern Old Aspen, between 10:00 and 16:30 (local time) during the period studied, originated from between 130° and 160° (19% of the time) and 280° and 340° (28% of the time), with 53% of wind vectors originating from other directions (Figure 2). The 80% probability density function of the total half-hourly CO_2 flux, determined using the footprint model parameterization [*Kljun et al.*, 2004], extended from between 300 m (highly convective) and 900 m (near neutral) conditions in the direction of the wind vector (at a measurement height of 39 m and an average zero plane displacement of ~10 m). In the cross-wind direction (at 80% probability density function), footprints extended to distances between ±50 m and ±200 m. The maximum probability of flux (x_{max}) occurred at distances between 70 m and a maximum of 236 m from the eddy covariance tower (average x_{max} = 82 m, for all flux measurements within the study period).

[23] At Upland Aspen, prevailing wind vectors originated from between 260° and 340°, 55% of the time, with highest frequencies (28% of total) between 280° and 300°. A second smaller peak in the frequency of wind origins occurred between 190° and 260° (accounting for 19% of the total) (Figure 2). The 80% probability density function of the total half-hourly flux extended from between 160 m and 600 m during highly convective and near neutral atmospheric conditions, respectively. In the cross-wind direction, footprints extended to distances between ±20 m and 115 m from the wind vector. x_{max} occurred at distances between 40 m and a maximum of 156 m (average distance of x_{max} = 78 m).

[24] Wind directions during footprint periods and over 24 h periods throughout June, July, and August did not vary greatly in origin or frequency at either Southern Old Aspen or Upland Aspen (Figures 2b and 2d).

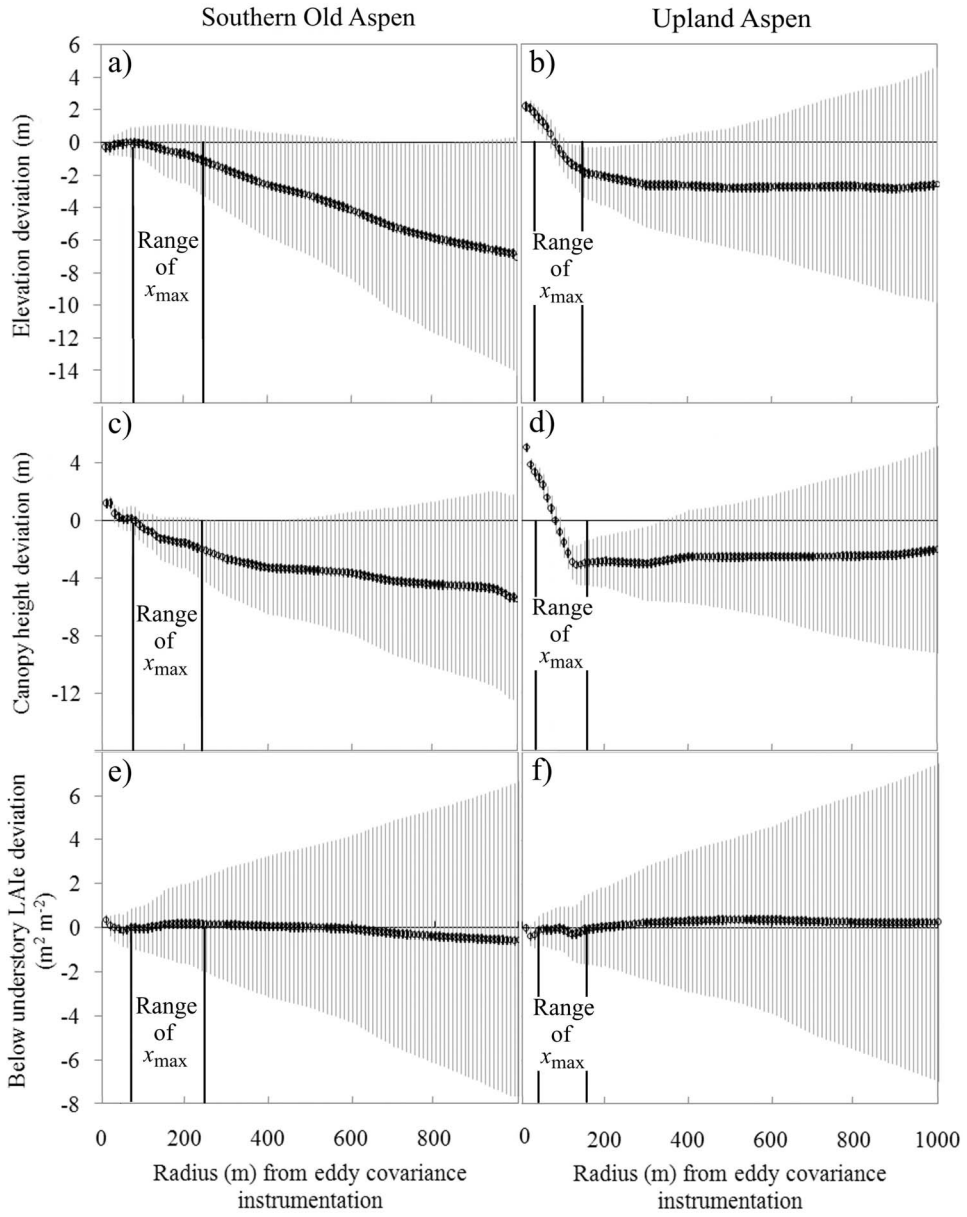

Figure 3. Site variability determined based on average and ±1σ (a, b) elevation, (c, d) canopy height, and (e, f) below understory (including canopy) LAIe at Southern Old Aspen and Upland Aspen, respectively. Deviation from zero is determined based on canopy structural and elevation differences at average footprint x_{max}, per site (82 m, Southern Old Aspen, and 78 m, Upland Aspen) compared with averages (and ±1σ) within 10 m radius increments in concentric rings centered on eddy covariance instrumentation. The temporal range of footprint x_{max} is also included to show area ranges of greatest sampling by eddy covariance.

5.2. Site Vegetation Structural and Topographical Characteristics

[25] Ground surface elevations at Southern Old Aspen within 1 km of the tower range from 541 to 571 m. This includes a southwest ridge that rises approximately 20 m above the surrounding terrain. Footprints originating from prevailing wind directions have, on average, taller trees (7%), higher $LAIe_{130}$ (30%), denser understory ($LAIe_{50}$ = 5%), and fewer low-lying areas compared with footprints originating from dominant southeasterly directions. Attributes are less than 6% different from the site average. At Upland Aspen, ground elevation varies between 638 m (southeast) and 680 m (northeast). Uplands rise 7 m to 21 m above the surrounding terrain. Prevailing wind vectors between 280° and 300° are characterized by shorter than average canopy heights (11%) reduced $LAIe_{50}$ (17%) and a greater proportion of low-lying areas.

[26] Figure 3 shows average vegetation structural and topographic variability with increasing (10 m radius) domain areas from eddy covariance instrumentation (±1σ as

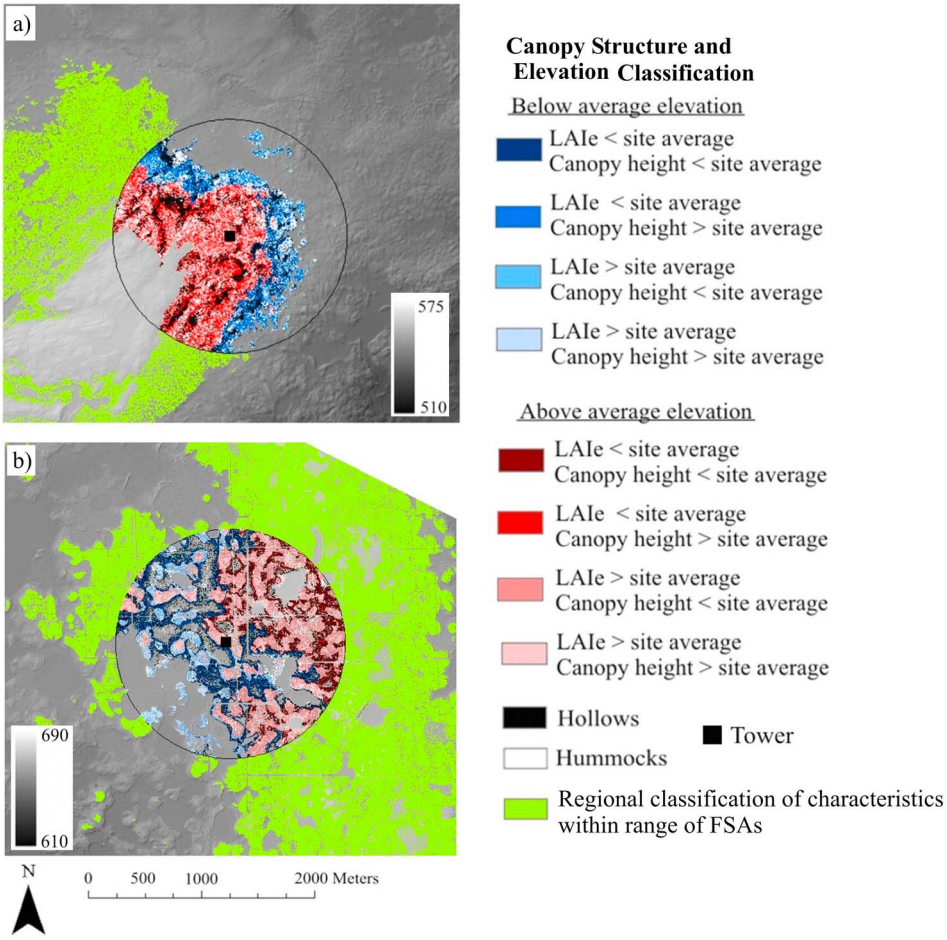

Figure 4. Classification of vegetation structure and topographical attributes within a 1 km radius of the eddy covariance instrumentation at (a) Southern Old Aspen and (b) Upland Aspen based on the footprint domain area originating from prevailing wind directions. Classified attributed ranges (Table 4) are grouped into above and below average elevation. Green sections represent areas that have the same range of vegetation structural and elevation characteristics found within the prevailing footprint domain area, applied to a 4 × 4 km area at each site. Graduated gray backgrounds represent elevation (m).

error bars). Elevation variability within the temporal range of footprint x_{max} varies by less than 1.5 m at Southern Old Aspen, and up to 6 m at Upland Aspen (Figures 3a and 3b). Negative elevation differences at distances greater than 220 m at Southern Old Aspen and within the range of footprint x_{max} at Upland Aspen indicate that both sites are located on uplands. Elevation σ increases with increasing distance, as expected, because of the integration of larger areas containing greater ranges of topographic attributes. At Upland Aspen, percentage area of uplands to lowlands is approximately equal at radii beyond 200 m.

[27] Canopy heights at Southern Old Aspen are greatest within rings closest to the tower but decrease with distance. This is caused by increased spacing between trees and the inclusion of shorter vegetation (between trees) in the canopy height model (Figures 3c and 3d). Average canopy heights do not vary greatly within the range of footprint x_{max} (average = 2 m, σ = 4m). At Upland Aspen, differences in average canopy heights between concentric rings and footprint x_{max} do not increase after ~150 m. The sharp difference in canopy heights within the range of footprint x_{max} at Upland Aspen is due to peatlands/wetlands located within 50 to 100 m eddy covariance instrumentation. Vegetation heights increase by up to 0.5 m on average from 300 m, because of upland aspen forests northeast of the tower.

[28] Average below canopy $LAIe_{50}$ varies by less than 0.3 m^2 m^{-2} at both sites, despite wide ranges of $LAIe_{50}$ estimated from lidar. At Southern Old Aspen, $LAIe_{50}$ is greatest within 20 m to 30 m of eddy covariance instrumentation, and decreases from between 30 m and 50 m because of canopy gaps. Unlike canopy height, $LAIe_{50}$ does not vary greatly from that at average footprint x_{max}. At Upland Aspen, a small reduction in average $LAIe_{50}$ (0.20) at 140 m to 170 m occurs because of peatlands, wetlands and ponds. These results indicate that lower than average elevation and canopy height biases exist beyond footprint x_{max} at both sites. This can have implications for flux sampling during periods of near-neutral atmospheric stability.

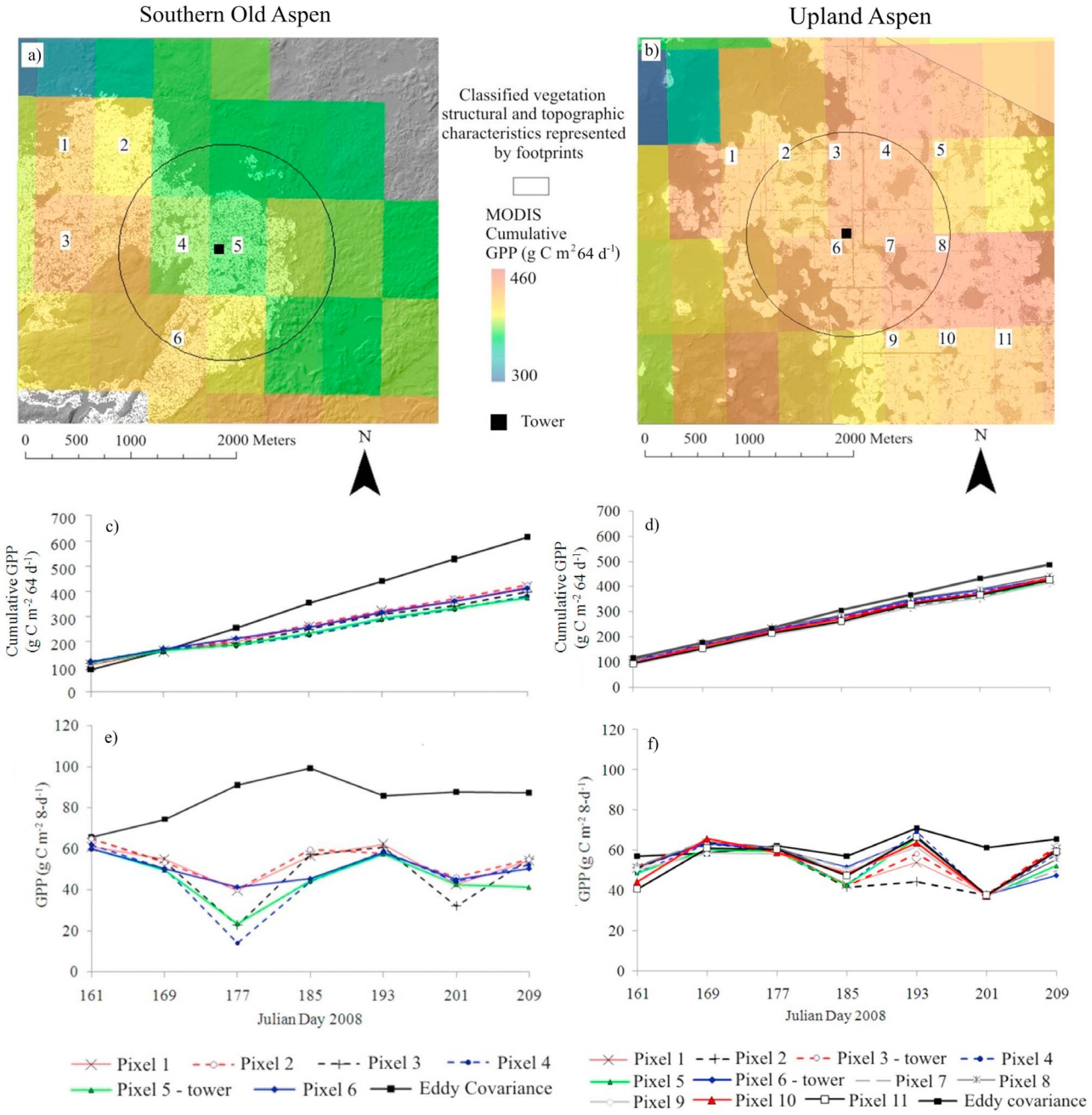

Figure 5. Semitransparent Moderate Resolution Imaging Spectroradiometer (MODIS) cumulative (DOY 161–209) gross primary production (GPP) georeferenced to the 4 × 4 km area surveyed by lidar at (a) Southern Old Aspen and (b) Upland Aspen. Numbered pixels have greater than 50% area coverage within 3-D attribute ranges sampled from prevailing wind directions by eddy covariance instrumentation. Eight-day cumulative GPP estimated from eddy covariance and MODIS are shown at (c) Southern Old Aspen and (d) Upland Aspen. Time series of 8 d cumulative GPP from MODIS and eddy covariance estimates at (e) Southern Old Aspen and (f) Upland Aspen.

5.3. Classification of Footprint Signatures: Site and MODIS Pixel Representation

[29] Figure 4 shows the results of the Boolean classification (defined in Table 4). Approximately 21% (Southern Old Aspen, Figure 4a) and 47% (Upland Aspen, Figure 4b) of the 4 × 4 km area surveyed by lidar were representative of structural characteristics within footprints from prevailing wind vectors. Within a 1 km radius area surrounding eddy covariance instrumentation, 56% (Southern Old Aspen) and 69% (Upland Aspen) of the area was within the range of

Table 5. Comparison Between GPP Estimated Using Eddy Covariance Methodology and Three MODIS Pixel Methods[a]

Comparison Statistic	Southern Old Aspen	Upland Aspen
MODIS Tower Pixel GPP		
r^2	0.81	0.69
Slope	0.53	0.85
RMSE	37.13	8.87
Average GPP of 3 × 3 *MODIS Pixels*		
r^2	0.71	0.69
Slope	0.53	0.84
RMSE	38.14	10.16
Average GPP of Footprint-Classified MODIS Pixels		
r^2	0.83	0.76
Slope	0.55	0.83
RMSE	37.12	8.47

[a]Comparison statistics include coefficient of variation (r^2), slope (intercept = 0), and root mean square error (RMSE) (g C m^{-2} 8 d^{-1}) (based on MODIS pixels with "very good" and "best possible" quality control flags).

attributes classified within footprints originating from prevailing wind directions.

[30] Figures 5a and 5b shows cumulative MODIS (pixels with >50% structural characteristics represented within footprints) and eddy covariance-estimated GPP over 8 d periods from DOY 161 to 209 at Southern Old Aspen and Upland Aspen. GPP estimated from cumulative gap-filled eddy covariance data at Southern Old Aspen in 2008 (DOY 161–209) was 614 gC m^{-2} 64 d^{-1} whereas MODIS estimated 319 gC m^{-2} 64 d^{-1} (Figure 5c). At Upland Aspen, eddy covariance estimates of GPP for the same period in 2006 was 486 gC m^{-2} 64 d^{-1} whereas MODIS estimated 434 gC m^{-2} d^{-1} (average pixels 3 and 6) (Figure 5d). Approximately 87% of the MODIS 'Southern Old Aspen tower' pixel is representative of site attributes sampled by eddy covariance instrumentation from prevailing wind directions. Pixels 2 and 3 (Figure 5a), have similar attributes and are less than 15% mixed. At Upland Aspen, the tower was located between two pixels (3, 6). These represented 80% and 71% of site attributes within flux footprints from prevailing wind directions, respectively. Other pixels, including 1, 9, and 10, have greater than 80% coverage of ranges of site attributes.

[31] Can the application of a footprint-based classification of vegetation structural and topographical characteristics improve the relationship between eddy covariance estimates of GPP and the MODIS GPP product? Table 5 shows coefficient of variation (r^2), the slope of the relationship (intercept = 0), and the root mean square error (RMSE) for relationships between eddy covariance estimated GPP and i) MODIS tower pixel GPP; ii) average GPP of 3 × 3 MODIS pixels, including the tower pixel; and iii) average GPP of MODIS pixels selected using the footprint-based classification.

[32] Classification of pixels based on within footprint three-dimensional land cover attributes from prevailing wind directions improves correlation between MODIS pixels and estimates of GPP from eddy covariance and meteorological instrumentation. However, average GPP from classified pixels is only marginally better than GPP estimated at the tower pixel (r^2 improves by 2% and 7% at Southern Old Aspen and Upland Aspen, respectively). Strong relationships between tower pixel GPP and eddy covariance-estimated GPP indicate that geolocation errors of tower pixels [e.g., *Wolfe et al.*, 2002] did not negatively influence GPP relationships because of similar land cover attributes beyond tower pixels. Relationships between average GPP of pixels identified using the footprint classification method and 3 × 3 MODIS pixels is a significant improvement at Southern Old Aspen (12% increased explanation of variance) because of land cover heterogeneity within north and southwest pixels, and a lesser improvement (7% increased explanation of variance) at Upland Aspen because of pixel similarity. This indicates that comparisons between larger area averaging of MODIS pixels (3 × 3, or, for example, 7 × 7 [*Heinsch et al.*, 2006], 25 × 25 [*Turner et al.*, 2006]) and eddy covariance estimates of GPP may reduce correspondence at some sites. If averaging over multiple pixels is required to obtain a more robust relationship, selection of nearby pixels based on land cover attributes sampled frequently by eddy covariance instrumentation as opposed to averaging between the nine MODIS pixels most proximal to the flux tower will likely improve relationships, however this requires further testing and may be site-specific.

5.4. Applying Confidence Limits to Within Site Sampling and MODIS Pixel Comparisons

[33] Cumulative frequency distributions of ground elevation, canopy height, and $LAIe_{50}$ footprint domain areas originating from prevailing, secondary peaks, and lesser sampled areas (Figure 2) are shown in Figure 6 at Southern Old Aspen and Upland Aspen. At Southern Old Aspen, footprints originating from wind directions between 130°–160° (19% of the time) have significantly different (p = 0.01) structural characteristics than those originating from prevailing wind directions (280°–340°, 28% of the time) because of greater spatial frequencies of shorter canopies and higher $LAIe_{50}$. Elevation characteristics vary greatly throughout the site (p = 0.01), because of a large ridge in the southwest part of the site, bogs, and low-lying hollows in the southeast. At Upland Aspen, attribute differences between footprints from prevailing wind directions (260°–340°, 55% of the time) and those originating from subdominant (340°–190°, 31%) and lower-frequency wind directions (190°–260°, 14%) did not have significantly different canopy heights (Figure 6). However, $LAIe_{50}$ differed significantly (p = 0.05) between prevailing wind directions from the northwest, and lower frequencies of footprints originating from south of the site. Differences were due to higher frequencies of short vegetation with high $LAIe_{50}$, located near ponds and in riparian areas west of the tower (Figure 6f). Elevation characteristics within different wind frequency domains were also significantly different (p = 0.01) because of locations of some ponds/wetlands, and low-lying/upland areas.

[34] Table 6 (Southern Old Aspen) and Table 7 (Upland Aspen) show confidence limits applied using a Kolmogorov-Smirnov test to differences in the spatial frequencies of vegetation structural (canopy height, $LAIe_{50}$) and elevation attributes found within a) MODIS pixels and b) wind direction footprint domains. At Southern Old Aspen, MODIS pixels 1 and 2 contain significantly different spatial

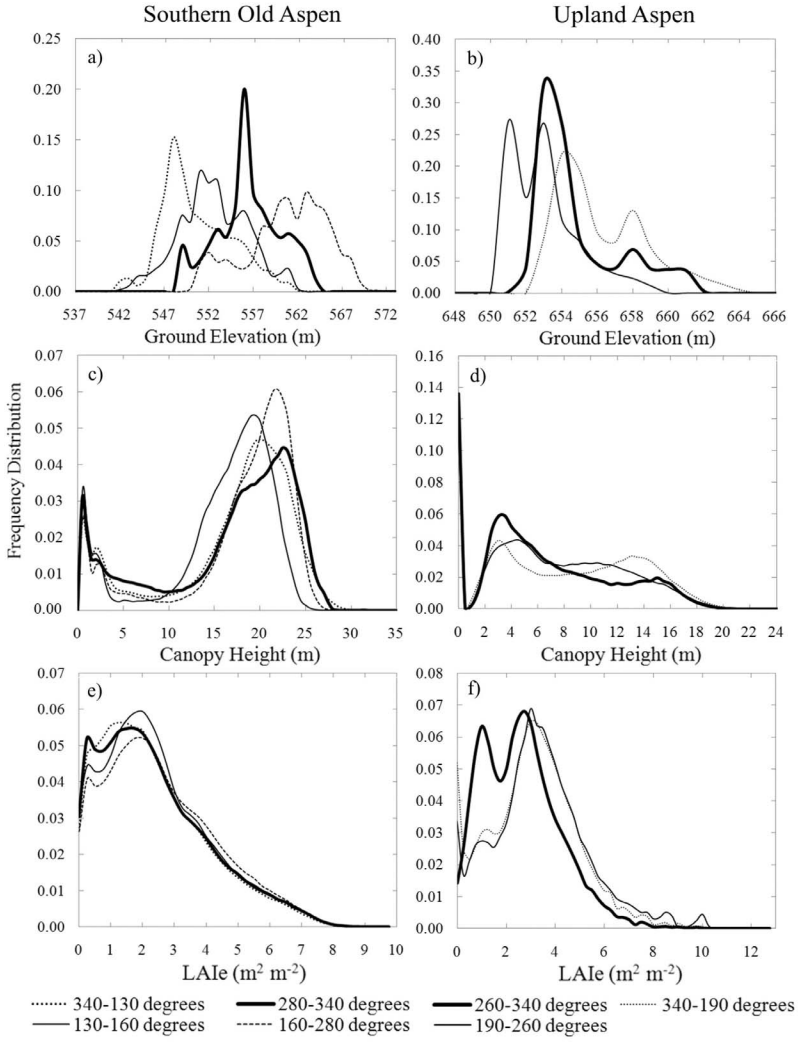

Figure 6. Frequency distributions of 3-D attributes (elevation, canopy height) and below understory LAIe at (a, c, e) Southern Old Aspen and (b, d, f) Upland Aspen. Cumulative frequency distributions derived from these curves (not shown) were used to test attribute differences within MODIS pixels.

frequencies of binned elevation, canopy heights, and $LAIe_{50}$, compared with that measured by eddy covariance instrumentation, from all footprint domains. Pixels 3, 4, and 5 (tower pixel) do not have significantly different attributes from those found within most footprint domains (excluding footprints originating from between 130 and 160 degrees); therefore H_0 cannot be rejected. Pixel 6 contains spatially similar frequencies of canopy height and $LAIe_{50}$ sampled from footprint areas originating from between 160° and 340° (sampled ~62% of the time by eddy covariance instrumentation). To this end, MODIS pixels 3, 4, and 5 are representative of eddy covariance instrument sampling 86% of the time, if elevation is excluded. If we choose average GPP from these three pixels to compare with GPP estimates from eddy covariance, the relationship improves slightly (r^2 = 0.85, slope = 0.55, RMSE = 37.25 g C m^{-2} 8 d^{-1}) when compared with average GPP using all footprint-classified pixels (Table 5). The frequency of elevations found within MODIS pixels are often very different from those sampled by eddy covariance instrumentation within footprint domains. Elevation may be a secondary driver of fluxes, whereby differences in vegetation structural characteristics, elevation, and soil moisture may autocorrelated to some extent. This needs to be explored further.

[35] At Upland Aspen, most MODIS pixels determined by the Boolean classification as having similar ranges of vegetation structural and elevation attributes as those found within prevailing wind directions, often do not have the same cumulative frequency of spatial canopy height or elevation attributes (Table 7). MODIS pixel 2 is most similar to footprint domains (sampled 46% of the time). Despite the differences in elevation and canopy height frequencies between MODIS pixels and footprint domain areas, $LAIe_{50}$ is not significantly different for 6 of 11 MODIS pixels examined. This may be an important consideration, as MODIS spectra are not directly sensitive to canopy height or topography (although canopy shadowing and soil wetness will have some influence on mixed pixel spectra). However, based on the average GPP of these six pixels, where $LAIe_{50}$ was the only similar attribute, relationships with eddy

Table 6. Kolmogorov-Smirnov Significance Levels (p Values) of Cumulative Frequency Differences Between 3-D Spatial Attributes Within Footprint Sampled Domain Areas (Originating From Clustered Wind Directions) and MODIS Pixels at Southern Old Aspen[a]

Wind Directions	P1	P2	P3	P4	P5	P6
DEM						
280–340	**0.01**	**0.01**	*>0.2*	**0.01**	*>0.2*	**0.01**
130–160	*>0.2*	*>0.2*	**0.01**	**0.01**	**0.01**	**0.01**
340–130	**0.01**	**0.01**	**0.01**	**0.01**	**0.01**	**0.01**
160–280	**0.01**	**0.01**	**0.01**	*>0.2*	**0.01**	*>0.2*
CHM						
280–340	**0.01**	**0.05**	*>0.2*	*>0.2*	*>0.2*	*>0.2*
130–160	**0.01**	**0.01**	**0.01**	**0.01**	**0.01**	**0.01**
340–130	**0.01**	0.1	*>0.2*	*>0.2*	0.15	**0.01**
160–280	**0.01**	*>0.2*	*>0.2*	*>0.2*	*>0.2*	*>0.2*
LAIe						
280–340	**0.05**	**0.05**	*>0.2*	*>0.2*	*>0.2*	*>0.2*
130–160	**0.01**	**0.01**	*>0.2*	*>0.2*	*>0.2*	*>0.2*
340–130	**0.01**	**0.01**	*>0.2*	*>0.2*	*>0.2*	*>0.2*
160–280	**0.01**	**0.01**	*>0.2*	*>0.2*	*>0.2*	*>0.2*

[a]DEM, elevation; CHM, canopy height; LAI–LAIe, below understory effective. Significance levels (p values) <0.05 (boldface) indicate that footprint domains have significantly different cumulative frequencies per structure type, whereas $p \geq 0.2$ (italics) show that these are not significantly different. P1, P2, etc., are defined in Figure 5.

covariance estimates of GPP were reduced ($r^2 = 0.60$, slope = 0.83, RMSE = 10.74) (Table 5).

6. Discussion

6.1. Site Structural Characteristics: Implications of Sampling During Near-Neutral Atmospheric Conditions

[36] *Kljun et al.* [2002, 2004] show that the shape of the footprint varies with atmospheric stability, whereby near-neutral atmospheric conditions result in a flattening of the footprint curve and increased footprint length. The opposite occurs during strongly convective periods. At Southern Old Aspen and Upland Aspen, increased convectivity results in sampling of canopy structural and topographic attributes closer to the tower. Increased stability results in sampling of other land cover types further from the tower, such as peatlands, wetlands, and low-lying areas. However, based on the sensitivity analysis performed on weighted versus unweighted footprints, the influence of landscape attributes located closer to the eddy covariance tower were not greatly different from those located further away from the tower, for most wind directions. Approximately 17% (Southern Old Aspen) and 26% (Upland Aspen) of 24 h u^* (June, July and August) measured using eddy covariance instruments occur during periods of stable stratification.

6.2. Site Representation and Scaling to MODIS Pixels

[37] In this study, MODIS underestimates GPP at both sites compared with eddy covariance estimates, however, the underestimation was greater at Southern Old Aspen than Upland Aspen. Differences between eddy covariance-estimated GPP and MODIS GPP could be due to atypical fluxes during the period of study that cannot be accounted for by the MODIS GPP algorithm, subsampling of specific characteristics within footprints by eddy covariance, mixed pixel influences on spectral responses, atmospheric constituents, geolocation errors, etc. [*Wolfe et al.*, 2002; *Heinsch et al.*, 2006; *Coops et al.*, 2007; *Chasmer et al.*, 2009]. At Southern Old Aspen cumulative gap-filled GPP during June, July, and parts of August 2008 (where data were available) was 8.3 gC m^{-2} d^{-1}, while average GPP from 1996 to 2009 for the same period was 7.8 gC m^{-2} d^{-1}. Minimum GPP was 6.3 gC m^{-2} d^{-1} (June, July, August) 2004, following three years of drought [*Kljun et al.*, 2006] and maximum GPP was 9.4 gC m^{-2} d^{-1} 2006, following two wet years. Unfortunately, temporal representation of GPP fluxes could not be assessed at Upland Aspen because fluxes were measured only during 2006.

[38] Subsampling of parts of the MODIS pixel within the eddy covariance field of view [*Turner et al.*, 2005; *Heinsch et al.*, 2006], especially from prevailing wind directions may not be entirely representative of the MODIS tower pixel in some cases. At Southern Old Aspen, footprints originating from prevailing wind directions encompassed large proportions of the tower pixel. This resulted in high correspondence between the tower pixel and measurements made by eddy covariance from prevailing wind directions, despite significant underestimation of GPP by MODIS at this site (Table 5). At Upland Aspen, footprints from prevailing wind directions often contained peatlands and wetlands, which had mixtures of shorter trees with low $LAIe_{50}$. MODIS tower pixels were slightly less representative of attributes measured from prevailing wind directions because of a mismatch in scale between (smaller) footprints and the area

Table 7. Kolmogorov-Smirnov Significance Levels (p Values) of Cumulative Frequency Differences Between 3-D Spatial Attributes Within Footprint Sampled Domain Areas (Originating From Clustered Wind Directions) and MODIS Pixels at Upland Aspen[a]

Wind Directions	P1	P2	P3	P4	P5	P6	P7	P8	P9	P10	P11
DEM											
260–340	**0.01**	**0.01**	**0.01**	**0.01**	**0.01**	*>0.2*	**0.01**	**0.01**	**0.01**	**0.01**	**0.01**
340–190	**0.01**	**0.01**	**0.01**	**0.01**	**0.01**	**0.01**	*>0.2*	**0.01**	**0.05**	**0.01**	**0.05**
190–260	**0.01**	**0.15**	**0.01**	**0.01**	**0.01**	**0.01**	**0.01**	**0.01**	**0.01**	**0.01**	**0.01**
CHM											
260–340	**0.01**	**0.01**	**0.01**	**0.01**	**0.01**	**0.01**	**0.01**	**0.01**	**0.01**	**0.01**	**0.01**
340–190	**0.01**	0.1	**0.01**	**0.01**	**0.01**	**0.01**	**0.01**	**0.01**	**0.01**	**0.01**	**0.01**
190–260	**0.01**	0.15	**0.01**	**0.01**	**0.01**	**0.01**	**0.01**	**0.01**	**0.01**	**0.01**	**0.01**
LAIe											
260–340	**0.01**	*>0.2*	*>0.2*	0.1	*>0.2*	**0.01**	*>0.2*	**0.01**	**0.01**	**0.01**	0.15
340–190	*>0.2*	**0.15**	*>0.2*	*>0.2*	*>0.2*	*>0.2*	*>0.2*	*>0.2*	*>0.2*	*>0.2*	*>0.2*
190–260	*>0.2*	**0.05**	*>0.2*	*>0.2*	*>0.2*	*>0.2*	*>0.2*	*>0.2*	*>0.2*	*>0.2*	*>0.2*

[a]DEM, elevation; CHM, canopy height; LAI–LAIe, below understory effective. Significance levels (p values) <0.05 (boldface) indicate that footprint domains have significantly different cumulative frequencies per structure type, whereas $p \geq 0.2$ (italics) show that these are not significantly different. P1, P2, etc., are defined in Figure 5.

contained within the MODIS tower pixels. This resulted in less explanation of variance by MODIS pixels, but also reduced differences between eddy covariance and MODIS estimates of GPP. MODIS often underestimates GPP in highly productive ecosystems and overestimates GPP in low-productivity sites [e.g., *Turner et al.*, 2005; *Heinsch et al.*, 2006; *Coops et al.*, 2007]. At Upland Aspen, there are relatively equal proportions of forested uplands, peatlands, and riparian areas which are averaged within MODIS pixels resulting in reduced biomass (determined from spectral vegetation indices) used in the MODIS GPP algorithm. Further, sampling of low-lying areas by eddy covariance instruments may have reduced 8 d cumulative GPP, making it more comparable to that of MODIS.

[39] High-frequency sampling by eddy covariance instrumentation of areas of hazelnut/aspen understory within footprints from prevailing wind directions at Southern Old Aspen may have also resulted in greater eddy covariance estimates of GPP when compared with MODIS GPP. The understory comprises of 39% of the total area within a 1 km radius of eddy covariance instrumentation (determined from airborne lidar), and is sampled approximately 26% of the time, over 24 h periods during June, July, and August. *Black et al.* [1996] and *Grant et al.* [1999] estimate that the understory at Southern Old Aspen sequesters approximately 60% of the C sequestered by the canopy. Therefore, sampling of areas that have this vigorous understory by eddy covariance instrumentation will likely increase GPP estimates when compared with MODIS pixel GPP.

[40] Is there an optimal pixel resolution that should be used for scaling fluxes measured by eddy covariance instrumentation? From the results of the MODIS pixel comparison with eddy covariance estimates of GPP (Table 5), we find that the use of low-resolution (1 km) MODIS pixel is adequate for scaling GPP variability throughout the growing season (despite significant underestimation of flux) at Southern Old Aspen. At this site, footprints originating from prevailing wind directions sample much of what the MODIS pixel observes. Slight within-pixel heterogeneity will be averaged both within the footprint and within the MODIS pixel, so long as small areas of heterogeneity (for example, wetlands and other features) do not significantly alter NEP measured by eddy covariance instrumentation. Selection of MODIS pixels containing the same attributes as that measured by eddy covariance from prevailing wind directions improves the explanation of variance of GPP at both sites when compared to using the tower pixel alone and the average of 3 × 3 MODIS pixels. Within heterogeneous ecosystems, use of higher resolutions may be more appropriate so that the distribution and influence of land cover types within footprints and lower-resolution MODIS pixels can be assessed [e.g., *Chasmer et al.*, 2009].

6.3. Implication for Research

[41] The idea that fluxes sampled by eddy covariance will be influenced, to some extent, by canopy structural and topographic characteristics is not new. Several studies have observed wind direction influences on NEP related to canopy structure [e.g., *Rannik et al.*, 2000; *Aubinet et al.*, 2001; *Scanlon and Albertson*, 2003; *Yoshio et al.*, 2005; *Chasmer et al.*, 2008a]. Further, meteorological driving mechanisms related to photosynthesis and respiration, are often affected by vegetation structure and topography [e.g., *Baldocchi et al.*, 1997; *Chen et al.*, 2002; *Griffis et al.*, 2003; *Gaumont-Guay et al.*, 2006; *Khomik et al.*, 2006; *Pomeroy et al.*, 2008]. Ecosystem structure, flux scalars, and the frequency of sampling of ecosystem parts by eddy covariance may have significant implications for satellite product evaluation [e.g., *Turner et al.*, 2006].

[42] The development and application of a new method for classifying vegetation structural and topographic characteristics observed by eddy covariance instrumentation (via the combination of a flux footprint model and lidar data) shows great promise for efficient comparisons between satellite vegetation products and eddy covariance-based estimates of vegetation production. The spatial frequency of land cover attributes within MODIS classified pixels were also compared with sampling of the same attributes found within various footprint wind direction domains using a Kolmogorov-Smirnov test. The application of this test provides users with an index of confidence that frequencies of 3-D attributes found within MODIS pixels are the same or different from those sampled by eddy covariance instruments. Where MODIS pixels do have similar attributes to those sampled by eddy covariance, additional confidence can be applied to temporal frequencies of eddy covariance sampling. For example, at Southern Old Aspen, MODIS pixels 3, 4, and 5 are representative of 3-D land cover attributes sampled by eddy covariance instruments 86% of the time. This will improve our understanding of the complex relationships between MODIS pixel GPP and that measured by eddy covariance instruments.

6.4. Improvements From Previous Integration Methods

[43] Several studies have indicated a need for remote sensing-based assessments of site heterogeneity for site selection [e.g., *Goulden et al.*, 2010] and eddy covariance representation [e.g., *Chen et al.*, 2011] using spectral vegetation indices. Spectral vegetation indices from moderate resolution satellites such as Landsat provide an excellent means for examining site heterogeneity, however in some cases, the cause for the pixel variability is unknown. For example, correlations between the normalized difference vegetation index and biophysical attributes vary between species types, seasons, years, and sensors [e.g., *Hall et al.*, 1995; *Chen*, 1996; *Franklin et al.*, 1997; *Eklundh et al.*, 2001; *Lu et al.*, 2004; *McMillan and Goulden*, 2008]. Spectral bands can be significantly affected by solar zenith angle [*Hall et al.*, 1995], shadowing and soil reflectance [*Treitz and Howarth*, 1999], stand structure [*Wang et al.*, 2005], and saturation of the normalized difference vegetation index at LAI > ~3.5 m^2 m^{-2} [*Fassnacht et al.*, 1997; *Wang et al.*, 2005]. This should not, however, exclude the use of spectral vegetation indices for examining site heterogeneity or eddy covariance instrument representation, but some caution is warranted. Airborne scanning lidar, on the other hand, provides direct measurements of canopy and understory structure, and topographical variability at high resolutions (nominally 1 m) and does not suffer from the same geometrical/optical problems of spectral systems. It should be noted, however, that lidar data sets have their own limitations, but are often not problematic within a wide range of forest ecosystems. Vegetation heights can be un-

derestimated within grassland and low-shrub environments where only one return is recorded [e.g., *Hopkinson et al.*, 2005] and within some forests where crown apices represent a small surface area. This results in the reflection of pulses from the sides of the crown as opposed to the very top [*Gaveau and Hill*, 2003]. Estimates of canopy fractional cover may be biased in dense canopies where laser returns cluster near the tops of trees [e.g., *Chasmer et al.*, 2006]. This can be especially problematic with earlier generation single- or dual-return lidar systems.

[44] Alternative methods for examining eddy covariance sampling representation within and beyond flux footprints should also consider other types of high-resolution spectral remote sensing data sets [e.g., *St-Onge et al.*, 2004]. Structural vegetation attributes, canopy morphology as a function of spectral reflectance and shadowing, canopy gaps, topographic variability from digitized topographic maps, etc., can also be used as layers within classifications similar to the classification methodology and Kolmogorov-Smirnov test used in this study. The degree to which high-resolution spectral data can mimic site characteristics measured using airborne lidar has been compared in a few studies [e.g., *Tickle et al.*, 2006; *Véga and St-Onge*, 2008] but should be explored further with respect to classifying areas sampled using eddy covariance instruments.

6.5. Limitations and Uncertainty

[45] 1. CO_2 measurement uncertainties by eddy covariance instrumentation occur during periods of stable atmospheric conditions, when transfers of CO_2 fluxes by nonturbulent exchanges are not detected by the eddy covariance. These limitations were reduced within the footprint analysis, and to some extent when estimating GPP (where $u^* > 0.2$ were used, and periods less than this were gap-filled). Other limitations include (1) assumption of near-neutral atmospheric stability; (2) an inability to consider the full complexity of the eddy covariance equations; (3) terrain influences [*Massman and Lee*, 2002]; and (4) energy balance closure [*Barr et al.*, 2006]. *Barr et al.* [2006] suggest that a correction to the energy balance may be applied to CO_2 fluxes in order to increase them relative to the percentage underestimated when the energy balance cannot be closed.

[46] 2. Footprint uncertainty in heterogeneous ecosystems, such as Upland Aspen, result in an inability to properly characterize the exact source/sink area measured by eddy covariance. Simple footprint models, such as the footprint parameterization used here [*Kljun et al.*, 2004] are confined to spatially homogeneous flow. Complex footprint models of *Kljun et al.* [2002], the basis for the footprint parameterization used in this study, can account for heterogeneity within the landscape. However, these models are not often applied over long time series data sets because they are computationally intensive.

[47] 3. Uncertainties in the location of source/sink areas, based on averaging all three-dimensional attributes within the footprint area, ignores weighting of attributes by the probability density function. A sensitivity analysis comparing weighted versus unweighted footprints does not greatly influence attributes averaged within the 80% footprints at these sites, however, this should be checked at other sites. Future studies will include weighting of topographical and structural attributes according to the probability density function. This would effectively tie the most important or influential attributes (e.g., local canopy height, area of understory cover, ratio of the area of uplands to lowlands) to measured fluxes, after the removal of influences from atmospheric driving mechanisms.

[48] 4. Roughness length (z_0) and zero plane displacement (d) were determined from lidar and averaged within 10° wind vectors, up to 100 m from the eddy covariance (area of greatest probability of flux).

[49] 5. MODIS pixel geolocation errors can increase uncertainty in the location of pixels and reflectance spectra used to estimate GPP [*Wolfe et al.*, 2002].

[50] 6. Soil characteristics such as soil moisture, soil type, and soil temperature were not included, but will have significant influences on the spatial variability of fluxes [*Gaumont-Guay et al.*, 2006]. Lidar topographical indices may be used with a radiative transfer model to estimate ground surface moisture and temperature regimes, but should be tested with measurements.

7. Conclusions

[51] The marriage of plot measurements with eddy covariance data and low-resolution remote sensing data products is particularly difficult because of differing spatial and temporal scales [*Heinsch et al.*, 2006; *Turner et al.*, 2006]. Yet these comparisons are required to assess global validity of satellite-based products. In this study, a Boolean classification of ranges of 3-D attributes found within footprints was used to classify within and beyond site vegetation structural and topographic variability found within MODIS pixels. Confidence limits were assigned on a per-MODIS pixel basis by comparing cumulative frequencies of binned 3-D attributes within pixels to those found within footprints originating from prevailing wind (and other domain) directions. The integration of lidar data with a footprint model for scaling to low-resolution MODIS pixels can have important implications for (1) vegetation structural and topographic influences on the variability of NEP sampled from wind scalars within footprints [*Chasmer et al.*, 2008a]; (2) identifying landscape features within footprint frequently sampled areas; (3) classifying the spatial patterns of landscape heterogeneity within and beyond the fetch of the eddy covariance instrumentation; and (4) evaluating the influence of spatial vegetation heterogeneity (patches) and eddy covariance sampling on lower-resolution remote sensing products such as those from MODIS.

[52] Airborne scanning lidar instruments are especially useful because they directly measure within and below canopy 3-D properties. Therefore, lidar data provide information that is the same as many plot or transect-level vegetation structure measurements [e.g., *Hopkinson et al.*, 2005; *Chasmer et al.*, 2008b], but samples the entire region surveyed. Despite the benefits of lidar for local to regional scaling, contracted data collections can be expensive. In recent years, however, lidar data collections have become more widespread within industry (e.g., forestry, oil and gas) and government agencies (e.g., Canadian Forestry Service, U.S. Department of Agriculture). This has enabled large-scale mapping of natural resources for monitoring and extraction purposes. Often, data are publicly available. Numerous eddy covariance flux tower sites have already

been surveyed by lidar at some point during their operation (e.g., >9 known sites in Canada, several in Europe, USA, Scandinavia, and Australia). If lidar data do not exist, the methods used in this study could be applied to less expensive high-resolution aerial photography, GIS data layers, or satellite imagery.

[53] **Acknowledgments.** The authors would like to acknowledge Fluxnet-Canada, the Canadian Carbon Program and the Boreal Ecosystem Research and Monitoring Sites (BERMS), and site technicians for Southern Old Aspen eddy covariance data. Funding for Southern Old Aspen site has been provided by CFCAS, NSERC, BIOCAP Canada, and the Climate Research Division of Environment Canada. Lidar data at Southern Old Aspen were obtained through a National Environment Research Council (NERC) UK grant to Natascha Kljun (grant NE/G000360/1). Lidar data at Southern Old Aspen were processed at the Applied Geomatics Research Group by Allyson Fox. Funding for research at Upland Aspen was provided by the HEAD2 NSERC–Collaborative Research and Development grant program (CRDPJ337273-06), Canadian Oilsands Network for Research and Development, Ducks Unlimited, Alberta-Pacific Forest Industries Inc., and the Forest Producers Association of Canada. Canadian Foundation for Innovation (CFI) grants were provided to Kevin Devito (infrastructure grant) and the Applied Geomatics Research Group, NS (Chris Hopkinson). Lidar data at Upland Aspen were subsidized by Optech Inc., Toronto. MODIS data were obtained from the Oak Ridge National Laboratory Distributed Active Archive Center (ORNS DAAC) and are available online at http://www.daac.ornl.gov/MODIS/modis.html. Finally, the authors would like to acknowledge helpful comments from two anonymous reviewers.

References

Amiro, B. D. (1998), Footprint climatologies for evapotranspiration in a boreal catchment, *Agric. For. Meteorol.*, *90*, 195–201, doi:10.1016/S0168-1923(97)00096-8.

Aubinet, M., B. Chermanne, M. Vandenhaute, B. Longdoz, M. Yernaux, and E. Laitat (2001), Long term carbon dioxide exchange above a mixed forest in the Belgian Ardennes, *Agric. For. Meteorol.*, *108*, 293–315, doi:10.1016/S0168-1923(01)00244-1.

Baldocchi, D. D. (2003), Assessing the eddy covariance technique for carbon dioxide exchange rates of ecosystems: Past, present and future, *Global Change Biol.*, *9*(4), 479–492, doi:10.1046/j.1365-2486.2003.00629.x.

Baldocchi, D. D., C. A. Vogel, and B. Hall (1997), Seasonal variation of carbon dioxide exchange rates above and below a boreal jack pine forest, *Agric. For. Meteorol.*, *83*, 147–170, doi:10.1016/S0168-1923(96)02335-0.

Barr, A. G., T. A. Black, E. H. Hogg, N. Kljun, K. Morgenstern, and Z. Nesic (2004), Inter-annual variability in the leaf area index of a boreal aspen-hazelnut forest in relation to net ecosystem production, *Agric. For. Meteorol.*, *126*, 237–255, doi:10.1016/j.agrformet.2004.06.011.

Barr, A. G., K. Morgenstern, T. A. Black, J. H. McCaughey, and Z. Nesic (2006), Surface energy balance closure by the eddy-covariance method above three boreal forest stands and implications for the measurement of CO_2 flux, *Agric. For. Meteorol.*, *140*, 322–337, doi:10.1016/j.agrformet.2006.08.007.

Bernier, P. Y., P. Bartlett, T. A. Black, A. Barr, N. Kljun, and J. H. McCaughey (2006), Drought constraints on transpiration and canopy conductance in mature aspen and jack pine stands, *Agric. For. Meteorol.*, *140*, 64–78, doi:10.1016/j.agrformet.2006.03.019.

Black, T. A., et al. (1996), Annual cycles of water vapour and carbon dioxide fluxes in and above a boreal aspen forest, *Global Change Biol.*, *2*, 219–229, doi:10.1111/j.1365-2486.1996.tb00074.x.

Brown, S. M., R. M. Petrone, C. Mendoza, and K. J. Devito (2010), Surface vegetation controls on evapotranspiration from a sub-humid Western Boreal Plain wetland, *Hydrol. Process.*, *24*, 1072–1085, doi:10.1002/hyp.7569.

Chasmer, L., C. Hopkinson, and P. Treitz (2006), Investigating laser pulse penetration of a conifer canopy through the integration of airborne and terrestrial lidar, *Can. J. Remote Sens.*, *32*(2), 116–125, doi:10.5589/m06-011.

Chasmer, L., N. Kljun, A. Barr, A. Black, C. Hopkinson, H. McCaughey, and P. Treitz (2008a), Vegetation structural and elevation influences on CO_2 uptake within a mature jack pine forest in Saskatchewan, *Canada, Can. J. For. Res.*, *38*, 2746–2761, doi:10.1139/X08-121.

Chasmer, L., C. Hopkinson, P. Treitz, H. McCaughey, A. Barr, and A. Black (2008b), A lidar-based hierarchical approach for assessing MODIS fPAR, *Remote Sens. Environ.*, *112*, 4344–4357, doi:10.1016/j.rse.2008.08.003.

Chasmer, L., C. Hopkinson, A. Barr, A. Black, H. McCaughey, and P. Treitz (2009), Scaling and assessment of GPP from MODIS using a combination of airborne lidar and eddy covariance measurements over jack pine forests, *Remote Sens. Environ.*, *113*, 82–93, doi:10.1016/j.rse.2008.08.009.

Chen, B., J. M. Chen, G. Mo, T. A. Black, and D. E. J. Worthy (2008), Comparison of regional carbon flux estimates from CO_2 concentration measurement and remote sensing based footprint integration, *Global Biogeochem. Cycles*, *22*, GB2012, doi:10.1029/2007GB003024.

Chen, B., et al. (2011), Assessing eddy-covariance flux tower location bias across the Fluxnet-Canada Research Network based on remote sensing and footprint modelling, *Agric. For. Meteorol.*, *151*, 87–100, doi:10.1016/j.agrformet.2010.09.005.

Chen, J. M. (1996), Evaluation of vegetation indices and a modified simple ratio for boreal applications, *Can. J. Remote Sens.*, *22*, 229–242.

Chen, J. M., S. G. Leblanc, J. Cihlar, R. L. Desjardins, and J. I. MacPherson (1999), Extending aircraft- and tower-based CO_2 flux measurements to a boreal region using a Landsat thematic mapper land cover map, *J. Geophys. Res.*, *104*(D14), 16,859–16,877, doi:10.1029/1999JD900129.

Chen, J., M. Falk, E. Euskirchen, K. T. Paw Uu, T. Suchanek, S. Ustin, B. Bond, K. Brosofske, N. Phillips, and R. Bi (2002), Biophysical controls of carbon flows in three successional Douglas-fir stands based on eddy-covariance measurements, *Tree Physiol.*, *22*, 169–177.

Coops, N. C., T. A. Black, R. S. Jassal, J. A. Trofymow, and K. Morgenstern (2007), Comparison of MODIS, eddy covariance determined and physiologically modeled gross primary production (GPP) in a Douglas-fir forest stand, *Remote Sens. Environ.*, *107*, 385–401, doi:10.1016/j.rse.2006.09.010.

Devito, K., I. Creed, T. Gan, C. Mendoza, R. Petrone, U. Silins, and B. Smerdon (2005), A framework for broad scale classification of hydrologic response units on the Boreal Plains: Is topography the last thing to think of?, *Hydrol. Process.*, *19*(8), 1705–1714, doi:10.1002/hyp.5881.

Eklundh, L., L. Harrie, and A. Kuusk (2001), Investigating relationships between Landsat ETM+ sensor data and leaf area index in a boreal conifer forest, *Remote Sens. Environ.*, *78*, 239–251, doi:10.1016/S0034-4257(01)00222-X.

Falge, E., et al. (2001), Gap filling strategies for defensible annual sums of net ecosystem exchange, *Agric. For. Meteorol.*, *107*, 43–69, doi:10.1016/S0168-1923(00)00225-2.

Fassnacht, K. S., S. T. Gower, M. D. MacKenzie, E. V. Nordheim, and T. M. Lillesand (1997), Estimating the leaf area index of north central Wisconsin forests using the Landsat thematic mapper, *Remote Sens. Environ.*, *61*, 229–245, doi:10.1016/S0034-4257(97)00005-9.

Ferone, J. M., and K. J. Devito (2004), Shallow groundwater–surface water interactions of pond-peatland complexes along a Boreal Plain landscape gradient, *J. Hydrol.*, *292*(1–4), 75–95, doi:10.1016/j.jhydrol.2003.12.032.

Finnigan, J. (2004), The footprint concept in complex terrain, *Agric. For. Meteorol.*, *127*, 117–129, doi:10.1016/j.agrformet.2004.07.008.

Finnigan, J. J., R. Clement, Y. Mahli, R. Leuning, and H. A. Cleugh (2003), A re-evaluation of long-term flux measurement techniques Part I: Averaging and coordinate rotation, *Boundary Layer Meteorol.*, *107*, 1–48, doi:10.1023/A:1021554900225.

Foken, T., and M. Y. Leclerc (2004), Methods and limitations in validation of footprint models, *Agric. For. Meteorol.*, *127*, 223–234, doi:10.1016/j.agrformet.2004.07.015.

Franklin, S. E., M. B. Lavigne, M. J. Deuling, M. A. Wulder, and E. R. Hunt Jr. (1997), Estimation of forest leaf area index using remote-sensing and GIS data for modeling net primary production, *Int. J. Remote Sens.*, *18*, 3459–3471, doi:10.1080/014311697216973.

Gaumont-Guay, D., T. A. Black, T. J. Griis, A. G. Barr, R. S. Jassal, and Z. Nesic (2006), Interpreting the dependence of soil respiration on soil temperature and water content in a boreal aspen stand, *Agric. For. Meteorol.*, *140*, 220–235, doi:10.1016/j.agrformet.2006.08.003.

Gaveau, D., and R. Hill (2003), Quantifying canopy height underestimation by laser pulse penetration in small footprint airborne laser scanning data, *Can. J. Remote Sens.*, *29*(5), 650–657, doi:10.5589/m03-023.

Göckede, M., et al. (2008), Quality control of CarboEurope flux data—Part 1: Coupling footprint analyses with flux data quality assessment to evaluate sites in forest ecosystems, *Biogeosciences*, *5*(2), 433–450, doi:10.5194/bg-5-433-2008.

Goulden, M. L., J. W. Munger, S.-M. Fan, B. C. Daube, and S. C. Wofsy (1996), Measurements of carbon sequestration by long-term eddy covariance: Methods and a critical evaluation of accuracy, *Global Change Biol.*, *2*, 169–182, doi:10.1111/j.1365-2486.1996.tb00070.x.

Goulden, M. L., A. M. S. McMillan, G. C. Winston, A. V. Rocha, K. L. Manies, J. W. Harden, and B. P. Bond-Lamberty (2010), Patterns of NPP, GPP, respiration, and NEP during boreal forest succession, *Global Change Biol.*, *17*(2), 855–871, doi:10.1111/j.1365-2486.2010.02274.x. [[Printed *17*(2), 2011.]

Grant, R. F., T. A. Black, G. den Hartog, J. A. Berry, H. H. Neumann, P. D. Blanken, P. C. Yang, C. Russell, and I. A. Nalder (1999), Diurnal and annual exchanges of mass and energy between an aspen-hazelnut forest and the atmosphere: Testing the mathematical model Ecosys with data for the BOREAS experiment, *J. Geophys. Res.*, *104*, 27,699–27,717, doi:10.1029/1998JD200117.

Griffis, T. J., T. A. Black, K. Morgenstern, A. G. Barr, Z. Nesic, G. B. Drewitt, D. Gaumont-Guay, and J. H. McCaughey (2003), Ecophysiological controls on the carbon balances of three southern boreal forests, *Agric. For. Meteorol.*, *117*, 53–71, doi:10.1016/S0168-1923(03)00023-6.

Gryning, S. E., A. Holtslag, J. S. Irwin, and B. Silversten (1987), Applied dispersion modeling based on meteorological scaling parameters, *Atmos. Environ.*, *21*, 79–89, doi:10.1016/0004-6981(87)90273-3.

Hall, F. G., Y. E. Shimabukuro, and K. F. Huemmrich (1995), Remote sensing of forest biophysical structure using mixture decomposition and geometric reflectance models, *Ecol. Appl.*, *5*, 993–1013, doi:10.2307/2269350.

Heinsch, F. A., et al. (2006), Evaluation of remote sensing based terrestrial productivity from MODIS using regional tower eddy flux network observations, *IEEE Trans. Geosci. Remote Sens.*, *44*(7), 1908–1925, doi:10.1109/TGRS.2005.853936.

Hopkinson, C., and L. Chasmer (2009), Testing a lidar intensity based model of canopy fractional cover across multiple forest ecozones, *Remote Sens. Environ.*, *113*, 275–288, doi:10.1016/j.rse.2008.09.012.

Hopkinson, C., L. Chasmer, G. Sass, I. Creed, M. Sitar, W. Kalbfleisch, and P. Treitz (2005), Assessing vegetation height and canopy volume in a boreal wetland complex using airborne scanning LiDAR, *Can. J. Remote Sens.*, *31*(2), 191–206, doi:10.5589/m05-007.

Kaimal, J. C., and J. Finnigan (1994), *Atmospheric Boundary Layer Flows: Their Structure and Measurement*, pp. 255–261, Oxford Univ. Press, New York.

Khomik, M., M. A. Arain, and J. H. McCaughey (2006), Temporal and spatial variability of soil respiration in a boreal mixedwood forest, *Agric. For. Meteorol.*, *140*, 244–256, doi:10.1016/j.agrformet.2006.08.006.

Kim, J., Q. Guo, D. Baldocchi, M. Leclerc, L. Xu, and H. Schmid (2006), Upscaling fluxes from tower to landscape: Overlaying flux footprints on high-resolution (IKONOS) images of vegetation cover, *Agric. For. Meteorol.*, *136*, 132–146, doi:10.1016/j.agrformet.2004.11.015.

Kljun, N., M. W. Rotach, and H. P. Schmid (2002), A three-dimensional backward Lagrangian footprint model for a wide range of boundary-layer stratifications, *Boundary Layer Meteorol.*, *103*, 205–226, doi:10.1023/A:1014556300021.

Kljun, N., P. Calanca, M. Rotach, and H. Schmid (2004), A simple parameterisation for flux footprint predictions, *Boundary Layer Meteorol.*, *112*, 503–523, doi:10.1023/B:BOUN.0000030653.71031.96.

Kljun, N., T. A. Black, T. J. Griffis, A. G. Barr, D. Gaumont-Guay, K. Morgenstern, J. H. McCaughey, and Z. Nesic (2006), Response of net ecosystem productivity of three boreal forest stands to drought, *Ecosystems*, *9*, 1128–1144, doi:10.1007/s10021-005-0082-x.

Lu, D., P. Mausel, E. Brondizio, and E. Moran (2004), Relationships between forest stand parameters and Landsat TM spectral responses in the Brazilian Amazon Basin, *For. Ecol. Manage.*, *198*, 149–167, doi:10.1016/j.foreco.2004.03.048.

Massman, W. J., and X. Lee (2002), Eddy covariance flux corrections and uncertainties in long-term studies of carbon and energy exchange, *Agric. For. Meteorol.*, *113*, 121–144, doi:10.1016/S0168-1923(02)00105-3.

McMillan, A. M. S., and M. L. Goulden (2008), Age-dependent variation in the biophysical properties of boreal forests, *Global Biogeochem. Cycles*, *22*, GB2023, doi:10.1029/2007GB003038.

Monteith, J., and M. Unsworth (1990), *Principles of Environmental Physics*, 2nd ed., Edward Arnold, New York.

Morrison, H., C. Hopkinson, L. Chasmer, and N. Kljun (2010), A GIS modeling routine to optimize lidar-based effective leaf area index values in a boreal forest watershed, in *IAHS Red Book, September 25, 2010*, 4 pp., IAHS Press, Jackson Hole, Wyo.

Nagy, M. T., I. A. Janssens, J. C. Yuste, A. Carrara, and R. Ceulemans (2006), Footprint-adjusted net ecosystem CO_2 exchange and carbon balance components of a temperate forest, *Agric. For. Meteorol.*, *139*(3–4), 344–360, doi:10.1016/j.agrformet.2006.08.012.

Oke, T. R. (1996), *Boundary-Layer Climates*, 2nd ed., Routledge, New York.

Petrone, R., U. Silins, and K. J. Devito (2007), Dynamics of evapotranspiration from a riparian pond complex in the Western Boreal Forest, Alberta, Canada, *Hydrol. Process.*, *21*, 1391–1401, doi:10.1002/hyp.6298.

Pomeroy, J., A. Rowlands, J. Hardy, T. Link, D. Marks, R. Essery, J. Sicart, and C. Ellis (2008), Spatial variability of shortwave irradiance for snowmelt in forests, *J. Hydrometeorol.*, *9*, 1482–1490, doi:10.1175/2008JHM867.1.

Rahman, A., J. Gamon, D. Fuentes, D. Roberts, and D. Prentiss (2001), Modeling spatially distributed ecosystem flux of boreal forest using hyperspectral indices from AVIRIS imagery, *J. Geophys. Res.*, *106*(D24), 33,579–33,591, doi:10.1029/2001JD900157.

Rannik, Ü., M. Aubinet, O. Kurbanmuradov, K. K. Sabelfeld, T. Markkanen, and T. Vesala (2000), Footprint analysis for measurements over a heterogeneous forest, *Boundary Layer Meteorol.*, *97*, 137–166, doi:10.1023/A:1002702810929.

Rebmann, C., et al. (2005), Quality analysis applied on eddy covariance measurements at complex forest sites using footprint modelling, *Theor. Appl. Climatol.*, *80*, 121–141, doi:10.1007/s00704-004-0095-y.

Running, S. W., R. R. Nemani, F. A. Heinsch, M. Zhao, M. Reeves, and H. Hashimoto (2004), A continuous satellite-derived measure of global terrestrial production, *BioScience*, *54*, 547–560, doi:10.1641/0006-3568(2004)054[0547:ACSMOG]2.0.CO;2.

Scanlon, T. M., and J. D. Albertson (2003), Water availability and the spatial complexity of CO_2, water, and energy fluxes over a heterogeneous sparse canopy, *J. Hydrometeorol.*, *4*, 798–809, doi:10.1175/1525-7541(2003)004<0798:WAATSC>2.0.CO;2.

Schmid, H. P. (1994), Source areas for scalars and scalar fluxes, *Boundary Layer Meteorol.*, *67*, 293–318, doi:10.1007/BF00713146.

Schmid, H. P. (2002), Footprint modeling for vegetation atmosphere exchange studies: A review and perspective, *Agric. For. Meteorol.*, *113*, 159–183, doi:10.1016/S0168-1923(02)00107-7.

Sellers, P., et al. (1997), BOREAS in 1997: Experiment overview, scientific results, and future directions, *J. Geophys. Res.*, *102*, 28,731–28,769, doi:10.1029/97JD03300.

Soegaard, H., C. Nordstroem, T. Friborg, B. U. Hansen, T. R. Christensen, and C. Bay (2000), Trace gas exchange in a high-Arctic valley: 3. Integrating and scaling CO_2 fluxes from canopy to landscape using flux data, footprint modeling, and remote sensing, *Global Biogeochem. Cycles*, *14*(3), 725–744, doi:10.1029/1999GB001137.

St-Onge, B., J. Jumelet, M. Cobello, and C. Véga (2004), Measuring individual tree height using a combination of stereophotogrammetry and lidar, *Can. J. For. Res.*, *34*(10), 2122–2130, doi:10.1139/x04-093.

Tickle, P. K., A. Lee, R. M. Lucas, K. Austin, and C. Witte (2006), Quantifying Australian forest floristics and structure using small footprint LiDAR and large scale aerial photography, *For. Ecol. Manage.*, *223*(1–3), 379–394, doi:10.1016/j.foreco.2005.11.021.

Treitz, P. M., and P. J. Howarth (1999), Hyperspectral remote-sensing for estimating biophysical parameters of forest ecosystems, *Prog. Phys. Geogr.*, *23*, 359–390.

Turner, D. P., S. Ollinger, M. L. Smith, O. Krankina, and M. Gregory (2004), Scaling net primary production to a MODIS footprint in support of Earth Observing System Product Validation, *Int. J. Remote Sens.*, *25*, 1961–1979, doi:10.1080/0143116031000150013.

Turner, D. P., et al. (2005), Site-level evaluation of satellite-based global terrestrial gross primary production and net primary production monitoring, *Global Change Biol.*, *11*, 666–684, doi:10.1111/j.1365-2486.2005.00936.x.

Turner, D. P., et al. (2006), Evaluation of MODIS NPP and GPP products across multiple biomes, *Remote Sens. Environ.*, *102*, 282–292, doi:10.1016/j.rse.2006.02.017.

Véga, C., and B. St-Onge (2008), Height growth reconstruction of a boreal forest canopy over a period of 58 years using a combination of photogrammetric and lidar models, *Remote Sens. Environ.*, *112*(4), 1784–1794, doi:10.1016/j.rse.2007.09.002.

Vesala, T., N. Kljun, Ü. Rannik, J. Rinne, A. Sogachev, T. Markkanen, K. Sabelfeld, T. Foken, and M. Y. Leclerc (2008), Flux and concentration footprint modelling: State of the art, *Environ. Pollut.*, *152*, 653–666, doi:10.1016/j.envpol.2007.06.070.

Vourlitis, G. L., W. C. Oechel, A. Hope, D. Stow, B. Boynton, J. Verfaillie Jr., Rommel Zulueta, and S. J. Hastings. (2000), Physiological models for scaling plot measurements of CO_2 flux across an Arctic tundra landscape, *Ecol. Appl.*, *10*, 60–72.

Wang, Q., S. Adiku, J. Tenhunen, and A. Granier (2005), On the relationship of NDVI with leaf area index in a deciduous forest site, *Remote Sens. Environ.*, *94*, 244–255, doi:10.1016/j.rse.2004.10.006.

Wolfe, R. E., M. Nishihama, A. Fleig, J. Kuyper, D. Roy, J. Storey, and F. S. Patt (2002), Achieving sub-pixel geolocation accuracy in support of MODIS land science, *Remote Sens. Environ.*, *83*, 31–49, doi:10.1016/S0034-4257(02)00085-8.

Yang, P. C., T. A. Black, H. H. Neumann, M. D. Novak, and P. D. Blanken (1999), Spatial and temporal variability of CO_2 concentration and flux in

a boreal aspen forest, *J. Geophys. Res.*, *104*, 27,653–27,661, doi:10.1029/1999JD900295.

Yoshio, I., M. Akira, M. Masami, N. Hideyuki, and O. Albert (2005), Spatial analysis of footprint effects on CO_2 flux measurements by eddy covariance method—A case study in rice paddy ecosystem, *Proc. Conf. Remote Sens. Soc. Jpn.*, *38*, 71–72.

Zhao, M., F. A. Heinsch, R. R. Nemani, and S. Running (2005), Improvements of the MODIS terrestrial gross and net primary production global data set, *Remote Sens. Environ.*, *95*, 164–176, doi:10.1016/j.rse.2004.12.011.

A. Barr, Environment Canada, National Water Research Institute, Saskatoon, SK S7N 3H5, Canada.

S. Brown, L. Chasmer, K. Giroux, and R. Petrone, Cold Regions Research Centre, Wilfrid Laurier University, Waterloo, ON N2L 3C5, Canada. (lechasme@yahoo.ca)

I. Creed, Department of Biology, University of Western Ontario, London, ON N6A 5B7, Canada.

K. Devito, Department of Biological Sciences, University of Alberta, Edmonton, AB T6G 2E9, Canada.

C. Hopkinson and T. Milne, Applied Geomatics Research Group, NSCC, Middleton, NS BOS 1P0, Canada.

N. Kljun, Department of Geography, College of Science, Swansea University, Swansea SA2 8PP, UK.